NASA MEMO 1-24-59L

NASA

MEMORANDUM

STATIC LIFT, DRAG, AND PITCHING-MOMENT CHARACTERISTICS OF WINGS WITH ARROW AND MODIFIED-DIAMOND PLAN FORMS COMBINED WITH SEVERAL DIFFERENT BODIES AT MACH NUMBERS OF 2.97, 3.35, AND 3.71

By Dennis F. Hasson and John G. Presnell, Jr.

Langley Research Center
Langley Field, Va.

CLASSIFIED DOCUMENT

This material contains information affecting the National Defense of the United States within the meaning of the espionage laws, Title 18, U.S.C., Secs. 793 and 794, the transmission or revelation of which in any manner to an unauthorized person is prohibited by law.

NATIONAL AERONAUTICS AND SPACE ADMINISTRATION

WASHINGTON

January 1959

[redacted]

NATIONAL AERONAUTICS AND SPACE ADMINISTRATION

MEMORANDUM 1-24-59L

STATIC LIFT, DRAG, AND PITCHING-MOMENT CHARACTERISTICS OF WINGS WITH ARROW AND MODIFIED-DIAMOND PLAN FORMS COMBINED WITH SEVERAL DIFFERENT BODIES AT MACH NUMBERS OF 2.97, 3.35, AND 3.71* **

By Dennis F. Hasson and John G. Presnell, Jr.

SUMMARY

Static lift, drag, and pitching-moment characteristics have been obtained at Mach numbers of 2.97, 3.35, and 3.71 for several wing-body combinations employing arrow- and modified-diamond-plan-form wings with about 70.3° of leading-edge sweep. The wings had uncambered, cambered, and cambered and twisted airfoil sections. The Reynolds numbers were approximately 2×10^6 and 3×10^6 for the wings with arrow- and modified-diamond plan forms, respectively. For arrow-wing configurations of the type tested, the uncambered wings led to greater maximum lift-drag ratios than did the wings with 20-percent leading-edge conical camber. All configurations tested were longitudinally stable throughout the test angle-of-attack and Mach number range. The static longitudinal stability parameter $\partial C_m/\partial C_L$ was almost invariant with Mach number.

INTRODUCTION

Several investigations have been made to develop configurations which will be aerodynamically efficient at supersonic speeds (e.g., refs. 1 to 3). A configuration with the fuselage situated entirely beneath the wing so that the wing and fuselage apexes were coincident was found to yield 15 percent higher values of maximum lift-drag ratio than a symmetrical model of the same volume. (See ref. 1.) The present paper reports

*Some of the material presented herein was included in a thesis entitled "An Analytical Method for Predicting Lift and Drag Characteristics of Flat-Top Wing-Body Combinations at Supersonic Speeds" submitted by Dennis F. Hasson in partial fulfillment of the requirements for the degree of Master of Science in Aeronautical Engineering, Virginia Polytechnic Institute, Blacksburg, Va., May 1958.

**Title, Unclassified.

[redacted]

the results of tests of similar configurations with both uncambered and cambered airfoils at Mach numbers of 2.97, 3.35, and 3.71. Also included are tests of these airfoils with a conventional fuselage. Although the configurations investigated were not specifically designed to yield high values of maximum lift-drag ratio, it was anticipated that the tests in which they were used would yield valuable information concerning the effect of fuselage interference and would give a comparison of cambered with uncambered airfoil sections.

SYMBOLS

The aerodynamic force and moment coefficients are referred to the stability axes. The reference center for the moment data was at 0.25 of the mean aerodynamic chord of the wing for all models. The symbols are defined as follows:

A	aspect ratio
A_b	base area, sq ft
b	wing span, in.
C_D'	drag coefficient, $\frac{D}{qS}$
$C_{D,b}'$	base drag coefficient, $\frac{-(C_{p,b})_{av}A_b}{S}$
C_L	lift coefficient, $\frac{L}{qS}$
C_{L_α}	lift-curve slope at $\alpha \approx 0^\circ$
C_m	pitching-moment coefficient, $\frac{\text{Pitching moment}}{qS\bar{c}}$
$C_{m,o}$	pitching-moment coefficient at $C_L = 0$
$\frac{\partial C_m}{\partial C_L}$	static longitudinal-stability parameter at $C_L \approx 0$
C_p	pressure coefficient, $\frac{p_l - p}{q}$
c	local chord, in.

$\bar{c}$	mean aerodynamic chord, in.
D	drag, lb
k	constant of proportionality
L	lift, lb
M	free-stream Mach number
p	free-stream static pressure, lb/sq ft
q	free-stream dynamic pressure, $0.7pM^2$, lb/sq ft
r	local radius of body of revolution, in.
S	wing area, sq ft
t	local thickness, in.
t/c	thickness ratio
x	distance along axis of revolution, in.
α	angle of attack (measured from reference planes shown in fig. 1), deg

Subscripts:

av	average value
b	base
l	local value
max	maximum value
min	minimum value

MODELS AND APPARATUS

Dimensional details and photographs of the models tested are presented in figures 1 and 2, respectively, and the geometric characteristics of the wings and bodies are given in table I.

For ease of reference, each of the models has been assigned a letter designation which will be used in the figures and throughout the text. The designations and distinguishing characteristics of the models are as follows:

Model designation	Body	Wing plan form	Camber	Leading-edge sweep, deg	A	t/c
B_1W_1 B_1W_2	Conventional fuselage	Arrow	None 20-percent L.E. (conical)	70.30	2	0.05
B_2W_1 B_2W_2	8.95° semicone	Arrow	None 20-percent L.E. (conical)	70.30	2	0.05
B_3W_3	3/4-power semibody	Modified diamond	None	70.35	1.3	0.03
B_4W_4	Small body of revolution	Modified diamond	Cambered and twisted	70.35	1.3	0.03

The 3/4-power semibody was derived from the equation $r = kx^{3/4}$, where k is a numerical constant, and the body was cut in half through the axis of revolution. The W_2 wing had 20-percent leading-edge conical camber with a design lift coefficient of 0.1. (See ref. 4.) The camber and twist of the W_4 wing were designed by the methods of reference 5 and were chosen to give minimum induced drag at a lift coefficient of 0.1 and a Mach number of 3.0. A sketch of the W_4 wing is shown in figure 3.

Since the ratio of base area to wing area for the B_2 and B_3 configurations was rather large, it would be expected that the base drag coefficients would be a considerable portion of the total drag coefficients. It therefore becomes of prime significance to measure accurately the pressures acting on the base of the models since the measured drag coefficients are to be adjusted to conditions corresponding to the free-stream static pressure at the model base (to be discussed subsequently). In order to determine the most accurate technique for measuring base pressures, three methods were employed on configuration B_2W_2. These methods consisted of (1) a flat base with five pressure tubes mounted 0.063 inch rearward of the base, (2) a plug mounted rearward of the flat base with four orifices measuring the pressure between the flat base and

plug as shown in figure 1(b), and (3) a recessed base with 32 pressure tubes as shown in figure 4. A discussion of the results of these tests may be found in the appendix. Only the recessed base was used on body B_3. (See fig. 5.) The ratio of base area to wing area for the B_1 and B_4 configurations was rather small, and a conventional method of measuring base pressure was used. This consisted of measuring the chamber pressure in the vicinity of the balance and the base pressures around the base annulus.

The tests were conducted in the high Mach number test section of the Langley Unitary Plan wind tunnel, which is a variable-pressure, continuous-flow tunnel. The test section is 4 feet square and approximately 7 feet long and is equipped with an asymmetric sliding-block nozzle which allows a continuous variation in Mach number from 2.3 to 4.65.

Forces and moments on the model were measured by means of a six-component internal strain-gage balance. This balance was attached by means of a sting to the tunnel central support system.

TESTS

The tests were conducted over an angle-of-attack range of -4° to 12° with a stagnation temperature of 150° F and a dewpoint of $<-30^\circ$ F. Other conditions were as follows:

Mach number	Stagnation pressure, lb/sq in. abs	Dynamic pressure, lb/sq ft.	Reynolds number based on $\bar{c}$	
			Arrow wings	Diamond wings
2.97	15.3	387	2.02×10^6	3.10×10^6
3.35	19.6	361	2.12	3.25
3.71	23.0	312	2.06	3.17

All tests were made with transition fixed at a constant 10 percent of the streamwise chord on the upper and lower surfaces of the wing. Transition was fixed by means of a 1/16-inch strip of No. 60 carborundum grains embedded in a plastic material which is sprayed on the surface of the wing. In addition a 1/16-inch strip was placed around the body at approximately 1/10 of the body length rearward of the nose.

[redacted]

CORRECTIONS AND ACCURACIES

The maximum deviation of local Mach number in the portion of the tunnel occupied by the model is ±0.015 from the average value given. The pressure gradients are sufficiently small to make a buoyancy correction unnecessary.

The average angularity of the flow in the region of the model was determined by comparing runs with the models upright and inverted, and the angles of attack were corrected accordingly. The angles of attack were also corrected for balance-sting deflections under static load and are estimated to be accurate to within $\pm 0.1^{\circ}$.

The drag data presented have been adjusted to conditions of free-stream static pressure at the base of the model. All drag adjustments were based on the average pressure coefficient acting at the base of the model. The values of base drag coefficient are presented in figure 6. The base drag coefficients of figure 6 for the B_2 configurations are for the body B_2 with a recessed base.

Based upon balance accuracy and repeatability of data, it is estimated that the measured quantities are accurate within the following limits:

C_L	±0.003
C_D'	±0.001
$C_{D,b}'$	±0.0005
C_m	±0.002
C_P	±0.005

PRESENTATION OF RESULTS

The results of this investigation are presented in the following figures:

	Figure
Variation of base drag coefficient with angle of attack for the various model configurations	6
Typical schlieren photographs of the various models	7
Longitudinal characteristics of B_1W_1 and B_1W_2	8
Longitudinal characteristics of B_2W_1 and B_2W_2	9

[redacted]

DISCUSSION OF RESULTS

Arrow-Plan-Form Wings

The variation of maximum lift-drag ratio with Mach number (fig. 10) shows the uncambered arrow-plan-form wing W_1 with either B_1 or B_2 to be more efficient at all test Mach numbers than the cambered wing W_2. For example, at $M = 2.97$ maximum lift-drag values for B_1W_1 and B_1W_2 models were 5.85 and 5.35, respectively, and at the same Mach number the $(L/D)_{max}$ values for B_2W_1 and B_2W_2 were 5.1 and 4.9, respectively. Correspondingly the minimum drag coefficients for the uncambered-wing configurations were lower than for the cambered-wing configurations.

An examination of the basic drag-characteristics plots (figs. 8 and 9) shows that the drag at $(L/D)_{max}$ for the cambered-wing configurations is greater than the drag at $(L/D)_{max}$ for the uncambered-wing configurations; thus the drag due to camber plus lift for the cambered-wing configuration is greater than the drag due to lift alone for the uncambered-wing configurations. The greater efficiency of the uncambered-wing configurations is reflected by this characteristic.

The effects of fuselage shape on the performance characteristics of the configurations cannot be analyzed since the bodies have no common parameters; however, these data indicate that the effects of camber on wing-body performance are essentially the same for two considerably different fuselage shapes at the test Mach numbers.

All the models with arrow-plan-form wings were longitudinally stable throughout the test angle-of-attack and Mach number range. The variation of the static-longitudinal-stability parameter $\partial C_m/\partial C_L$ was less than 3 percent of the mean aerodynamic chord throughout the test Mach number range for any given configuration. The lift-curve slope for all configurations with arrow-plan-form wings decreased with increasing Mach number, as would be expected.

Modified-Diamond-Plan-Form Wings

The configurations with modified-diamond-plan-form wings B_3W_3 and B_4W_4 are not comparable and are included only to show the general characteristics of these types of configurations. In any analysis of the data presented in figures 11 and 12, it should be pointed out that the angle-of-attack reference line of the two configurations is different. The highest value of maximum lift-drag ratio obtained in the present investigation, 6.7 at a Mach number of 2.97, was obtained with the B_4W_4 model.

The B_3W_3 and B_4W_4 models were longitudinally stable throughout the test angle-of-attack and Mach number range. The static longitudinal stability parameters were almost invariant with Mach number for both configurations. The lift-curve slopes of the two configurations showed the usual decrease with increasing Mach number.

CONCLUDING REMARKS

For the configurations with arrow-plan-form wings of the type tested, uncambered wings led to greater maximum lift-drag ratios than did wings with 20-percent leading-edge conical camber. All configurations tested were longitudinally stable throughout the test angle-of-attack and Mach number range. The static longitudinal-stability parameter $\partial C_m/\partial C_L$ was almost invariant with Mach number.

Langley Research Center,
National Aeronautics and Space Administration,
Langley Field, Va., October 14, 1958.

[redacted]

APPENDIX

A COMPARISON OF TECHNIQUES FOR MEASURING BASE PRESSURE

As previously mentioned, the techniques used to determine an accurate method of measuring base pressures on bodies such as B_2 consisted of (1) orifice instrumentation of a flat base, (2) orifice instrumentation of a plug at the base, and (3) orifice instrumentation of a recessed base. The first and third methods do not add anything to the test system that can change the flow phenomena at the base of the model. A plug at the base, however, changes the flow conditions at the base. In the past, the plug system has been used with cylindrical afterbodies, and for small angles of attack (in the range of this report) it has yielded accurate values of base drag coefficient; however, the plug generally had some small effect on lift coefficient and $C_{m,o}$. This system, however, was included to determine its accuracy with a noncylindrical-base configuration. Typical base pressure coefficients obtained with the various techniques are shown in the following table for the B_2W_2 model at $M = 2.97$ and $\alpha = 2.4^\circ$:

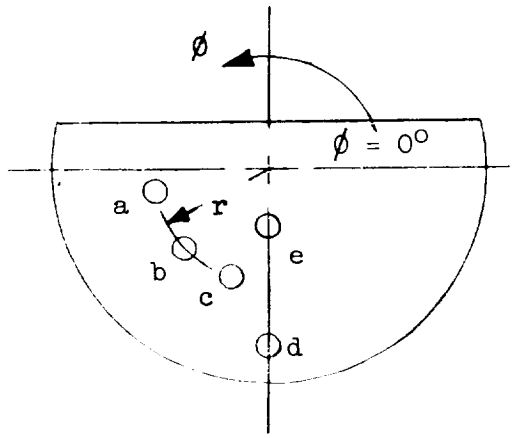

Orifice	r, in.	ϕ, deg	$C_{p,b}$
Recessed base			
a	2.00	180.0	-0.107
b	2.00	202.5	-.107
c	2.00	247.5	-.108
d	2.35	270.0	-.105
e	.50	270.0	-.104
Flat base			
a	2.18	183.0	-0.125
b	2.00	213.5	-.133
c	1.90	249.0	-.112
d	2.32	270.0	-.114
e	.60	270.0	-.078
Flat base with plug			
a	2.18	183.0	0.0288
b	2.00	213.5	.0231
c	1.90	249.0	.0371
d			
e	.60	270.0	.0116

The data presented in the table show that only the configuration with the recessed cavity has essentially the same pressure at every point on the base. The other base-pressure measuring techniques show fairly large variations in the pressure at the base and thus would require more instrumentation to define accurately the average pressure coefficient on the base. Furthermore, the flat base with plug technique is seen to cause a shift in $C_{m,o}$ similar to that of the cylindrical-afterbody tests previously mentioned; however, in this particular instance the shift in $C_{m,o}$ is only slight. The change in the basic stability characteristics for the model may lead to a false interpretation of the airplane trim characteristics and this possibility makes the plug method of measuring model base pressures even more unattractive.

In summation, it is seen that, for ease in instrumentation and for accuracy of test results, the recessed-base technique is the more desirable for wind-tunnel model tests.

[redacted]

REFERENCES

1. Eggers, A. J., Jr., and Syvertson, Clarence A.: Aircraft Configurations Developing High Lift-Drag Ratios at High Supersonic Speeds. NACA RM A55L05, 1956.

2. Syvertson, Clarence A., Wong, Thomas J., and Gloria, Hermilo R.: Additional Experiments With Flat-Top Wing-Body Combinations at High Supersonic Speeds. NACA RM A56I11, 1957.

3. Jorgensen, Leland H.: Experimental Lift-Drag Ratios for Two Families of Wing-Body Combinations at Supersonic Speeds. NACA RM A58A08, 1958.

4. Boyd, John W., Migotsky, Eugene, and Wetzel, Benton E.: A Study of Conical Camber for Triangular and Sweptback Wings. NACA RM A55G19, 1955.

5. Ginzel, I., and Multhopp, H.: Wings With Minimum Induced Drag in Supersonic Flow. Eng. Rep. No. 9937-M, The Glenn L. Martin Co., Aug. 1957.

[redacted]

[redacted]

TABLE I.- GEOMETRIC CHARACTERISTICS OF BODIES AND WINGS

Body

B_1:

Length, in.	28.825
Maximum diameter, in.	3.80
Fineness ratio	8.19

B_2:

Length, in.	20.730
Semivertex angle, deg	8.95
Maximum diameter, in.	6.53
Fineness ratio	3.16

B_3:

Length, in.	26.705
Maximum diameter, in.	5.84
Fineness ratio	4.57

B_4:

Length, in.	26.705
Maximum diameter, in.	2.50
Fineness ratio	10.68

Wing

W_1:

Area, sq ft	1.125
Span, in.	18.00
Mean aerodynamic chord, in.	12.00
Aspect ratio	2.00
Root chord, in.	18.00
Tip chord, in.	0
Taper ratio	0
Leading-edge sweep, deg	70.30
Airfoil section	Biconvex
Maximum thickness, percent	5

W_2:

Same geometric characteristics as wing W_1 with the exception of the following:

Modified NACA 65-series sections with 20-percent leading-edge conical camber (design $C_L = 0.1$) from 0 to 0.5c and biconvex sections from 0.5c to 1.0c.

Maximum thickness (located at 0.5c), percent	4.75

W_3:

Area, sq ft	1.716
Span, in.	17.92
Mean aerodynamic chord, in.	18.387
Aspect ratio	1.3
Root chord (theoretical), in.	27.58
Tip chord, in.	0
Taper ratio	0
Leading-edge sweep, deg	70.35
Airfoil section:	
0 to 0.5c	Modified NACA 65 Series
0.5c to 1.0c	Biconvex
Maximum thickness (located at 0.5c), percent	3

W_4:

Same geometric characteristics as wing W_3. For camber and twist see text.

[redacted]

[redacted]

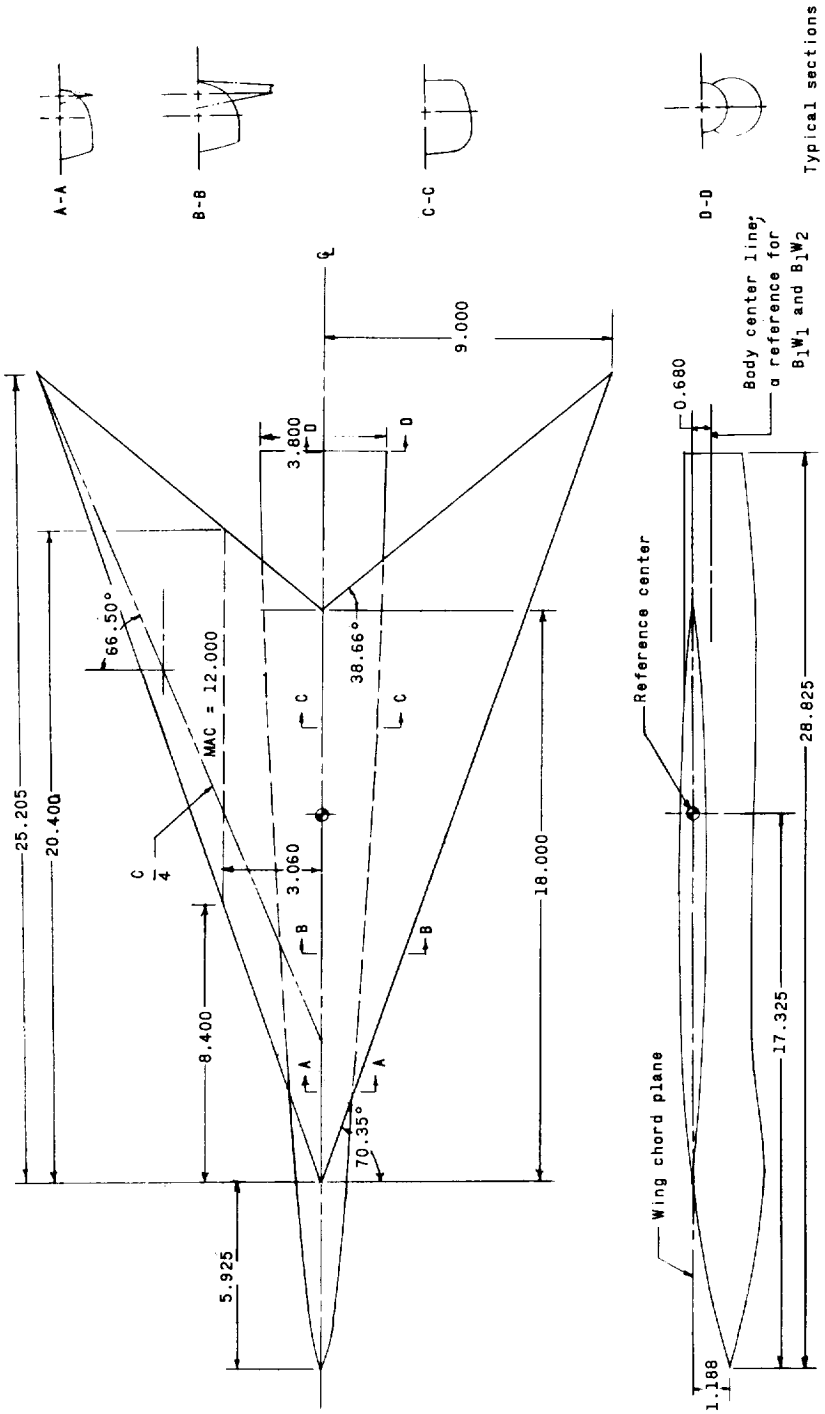

(a) Three-view drawing of B_1W_1.

Figure 1.- Model drawings. Dimensions are in inches unless otherwise noted.

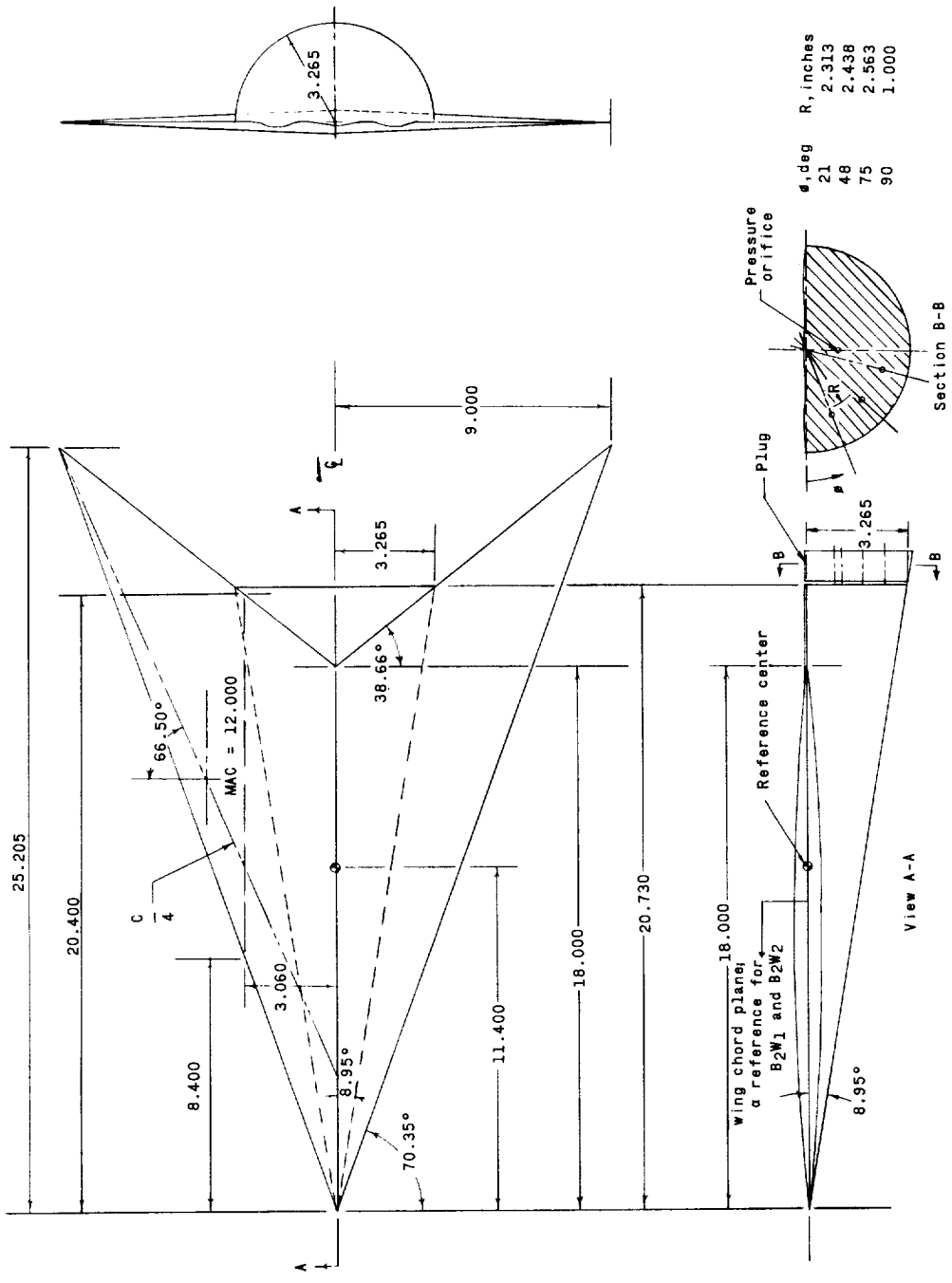

(b) Three-view drawing of B_2W_1.

Figure 1.- Continued.

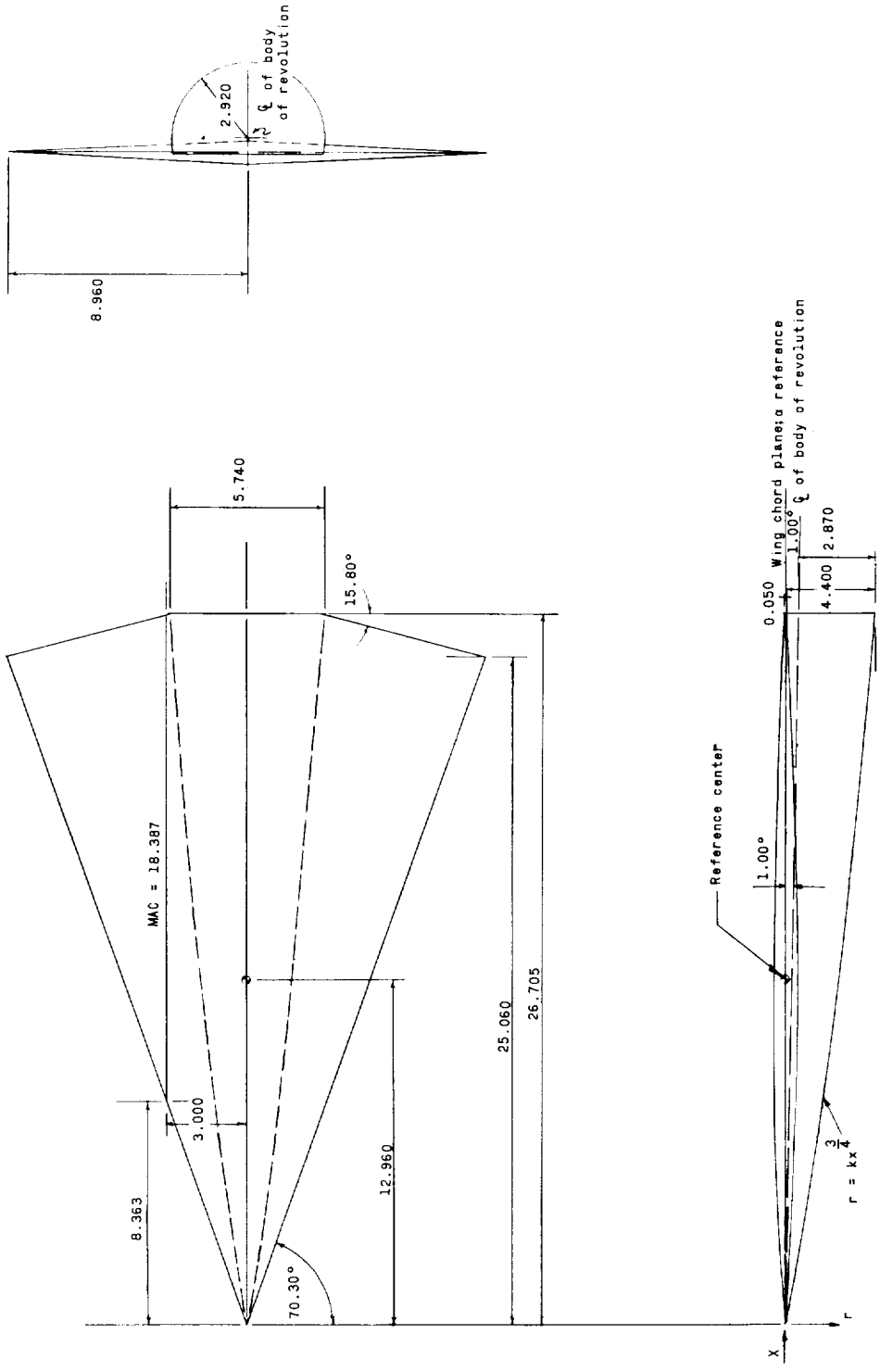

(c) Three-view drawing of B_3W_3.

Figure 1.- Continued.

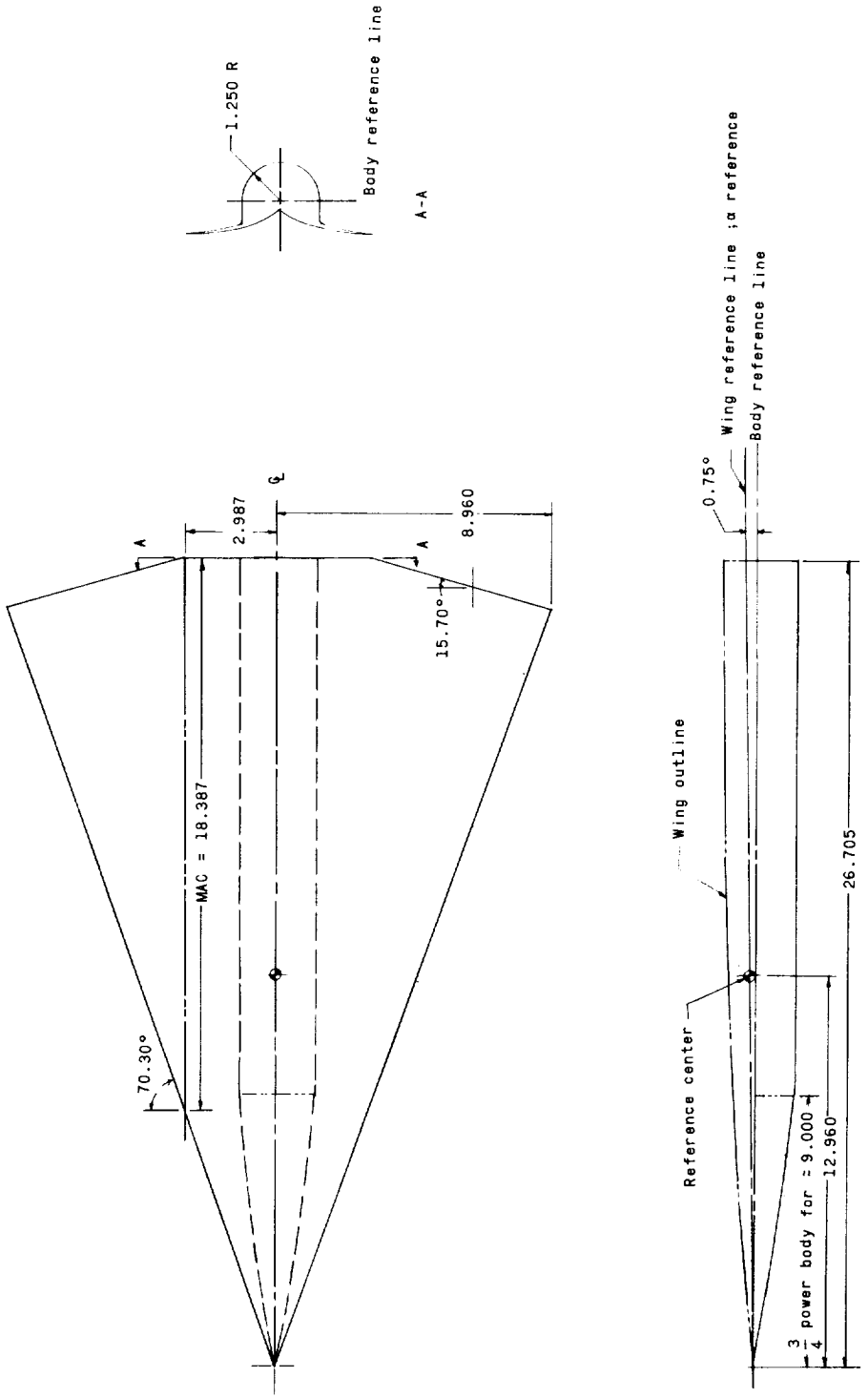

(d) Three-view drawing of B_4W_4.

Figure 1.- Concluded.

(a) Model B_1W_2. L-58-120a

Figure 2.- Photographs of the various models.

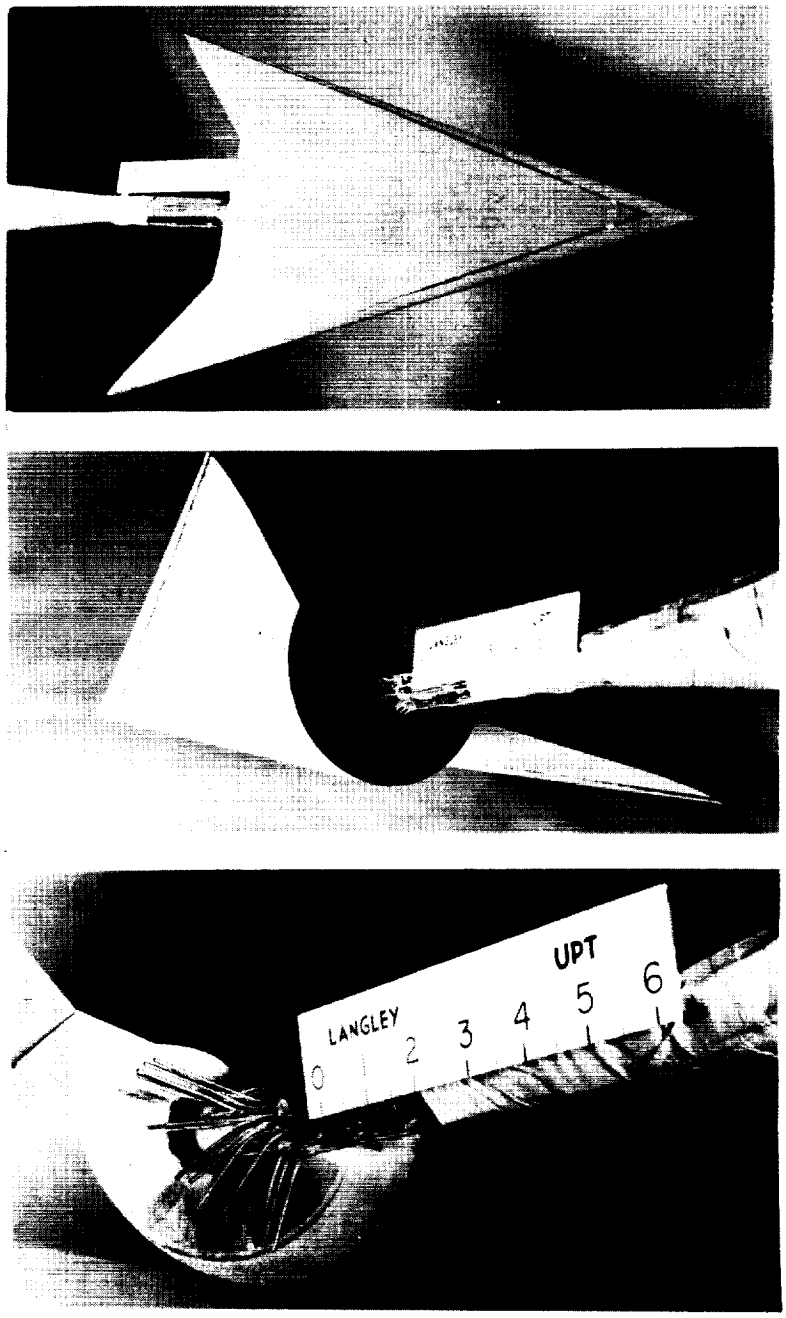

(b) Model B_2W_2. L-58-121a

Figure 2.- Continued.

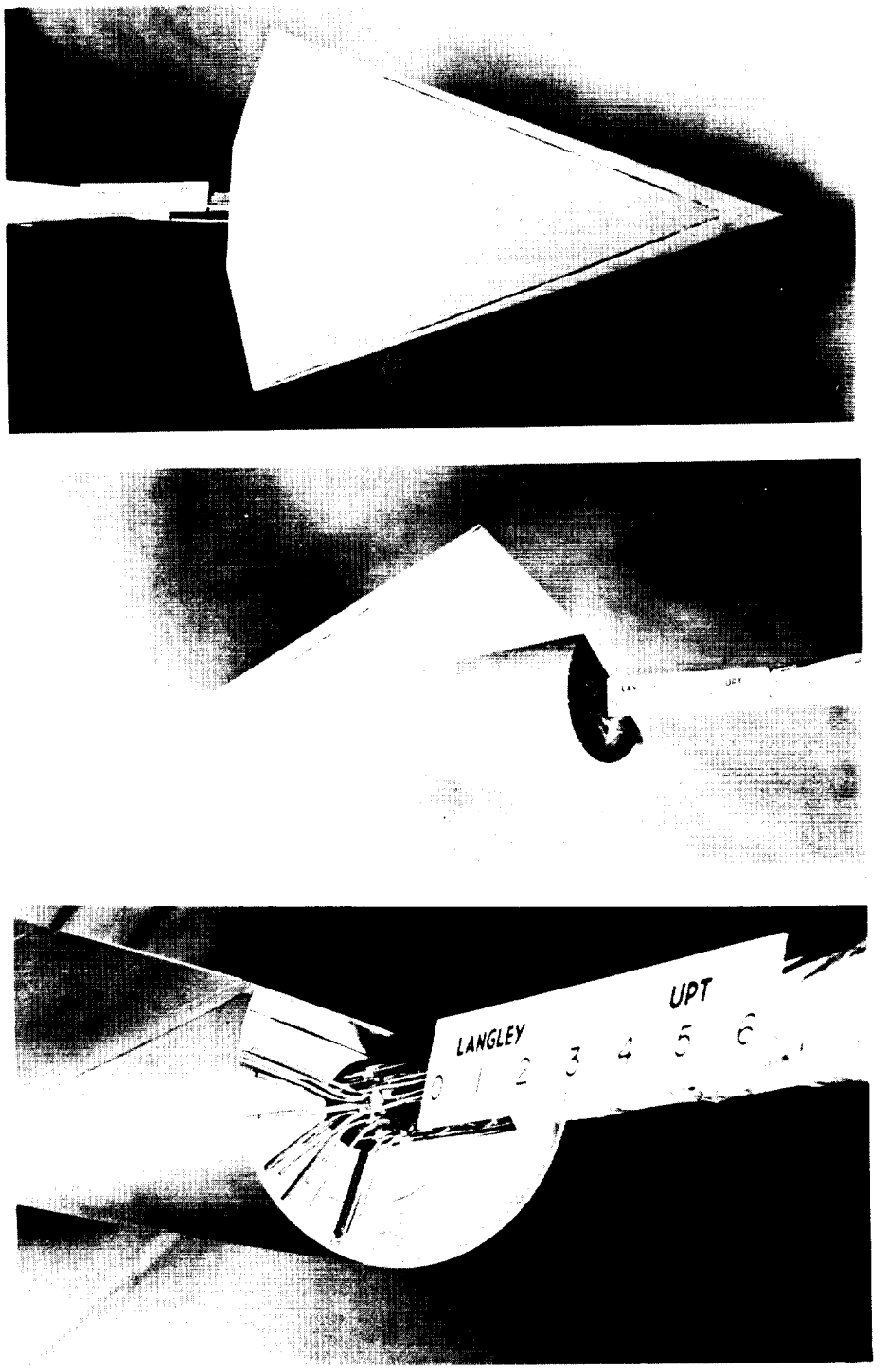

(c) Model B_3W_3. L-58-122a

Figure 2.- Continued.

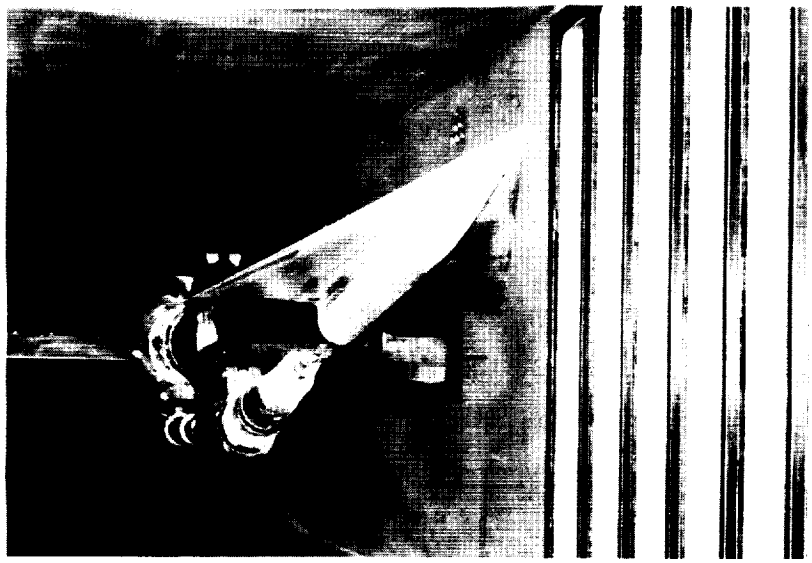

L-57-5286

L-57-5287

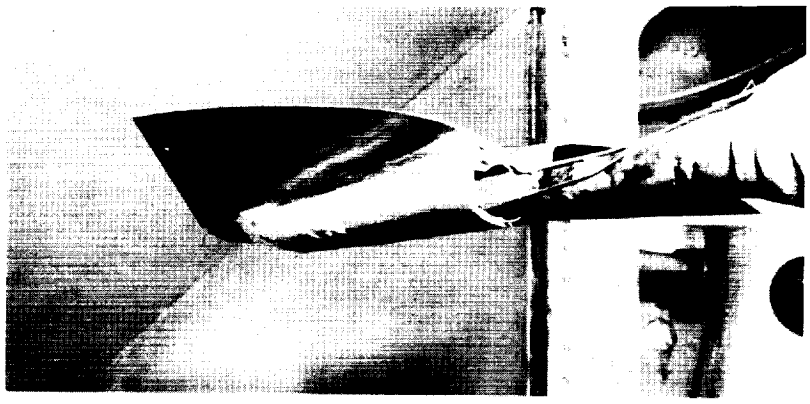

(d) Model B_4W_4. L-57-5291

Figure 2.- Concluded.

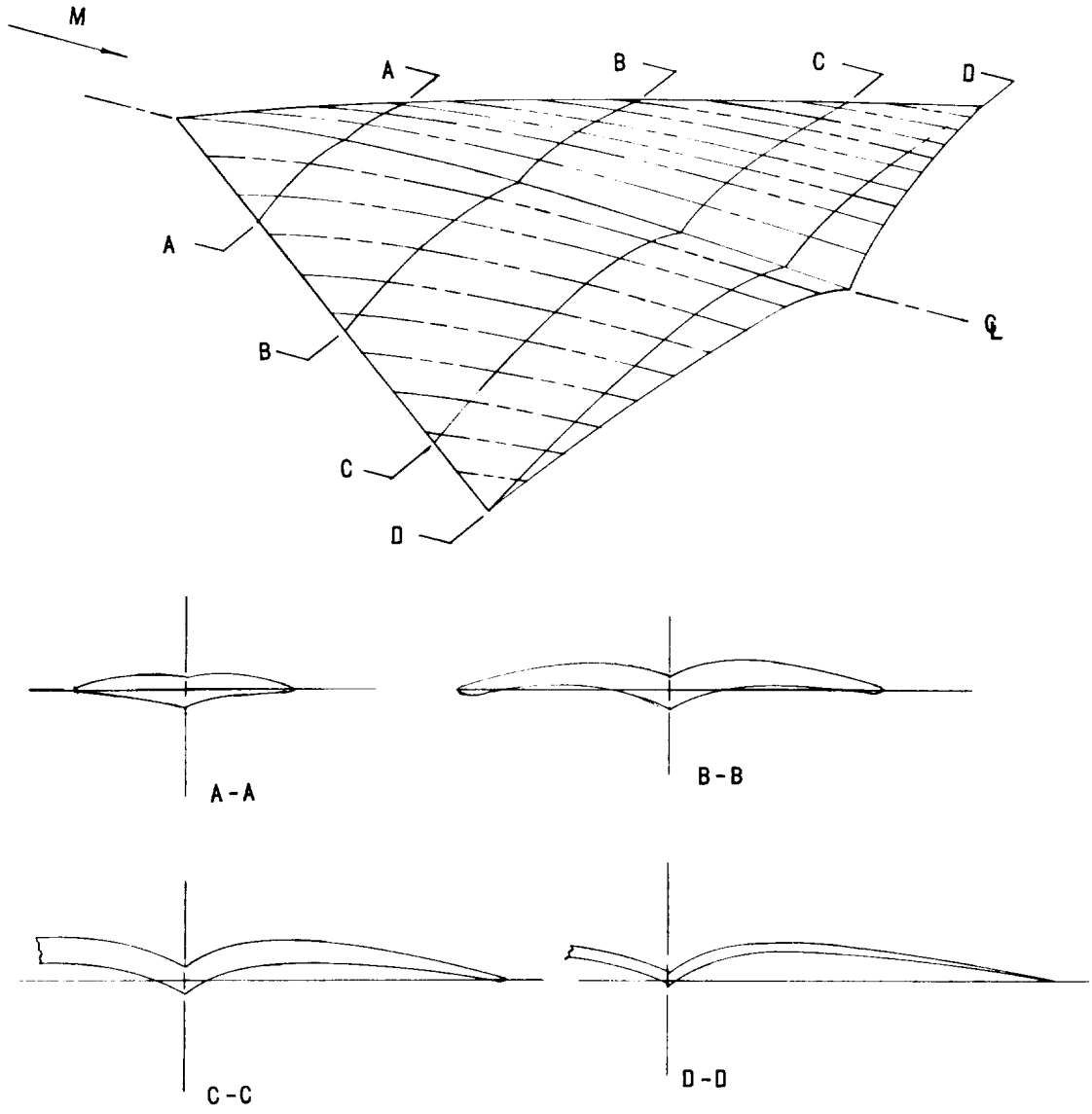

Figure 3.- Sketch of cambered and twisted diamond wing (W_4).

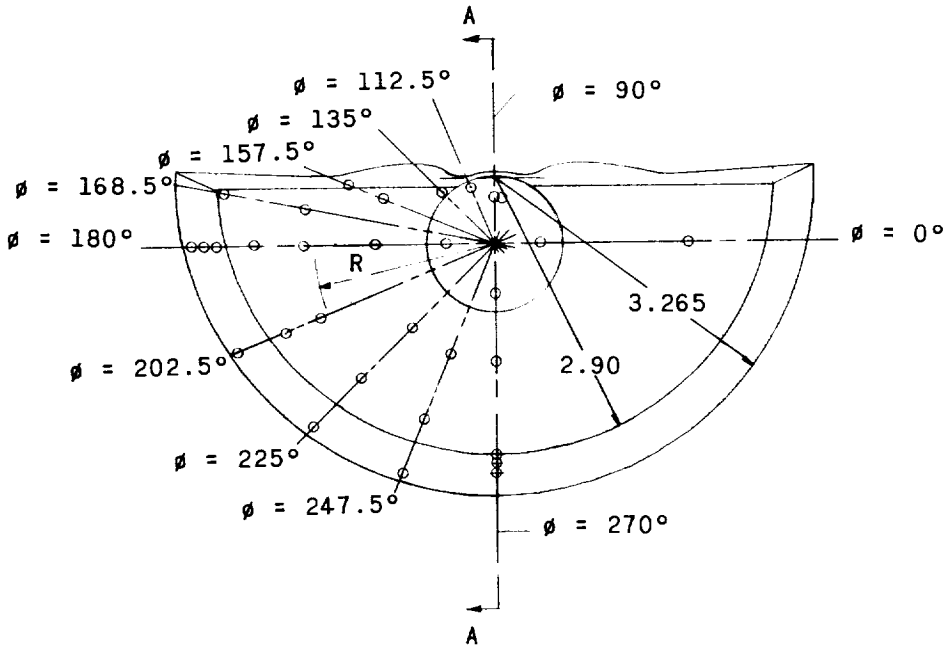

Orifice Locations

Orifice	ø, deg	R, in.
1	0	0.50
2	0	2.00
3	90	.50
4	90	.50
5	112.5	.63
6	135	.75
7	157.5	1.25
8	157.5	1.88
9	168.5	2.00
10	168.5	2.88
11	180	.50
12	180	1.25
13	180	2.00
14	180	2.50
15	180	2.90
16	180	3.05
17	180	3.20
18	202.5	2.00
19	202.5	2.38
20	202.5	2.95
21	225	1.25
22	225	2.00
23	225	2.70
24	247.5	1.25
25	247.5	2.00
26	247.5	2.60
27	270	.50
28	270	1.25
29	270	2.00
30	270	2.25
31	270	2.35
32	270	2.45

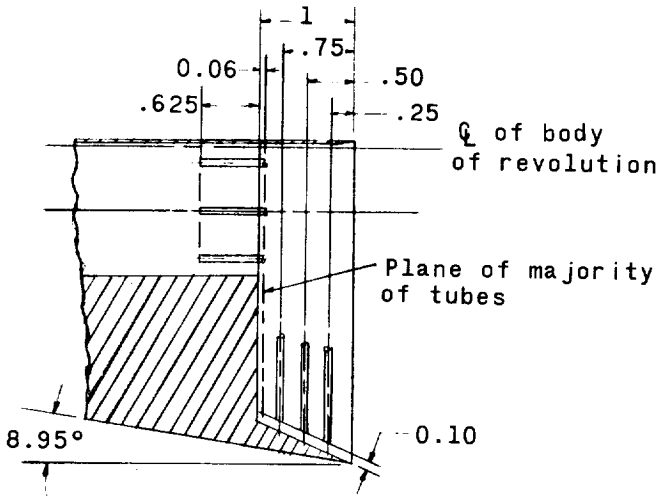

A-A

Figure 4.- Details of the base of body B_2. Dimensions are in inches unless otherwise noted.

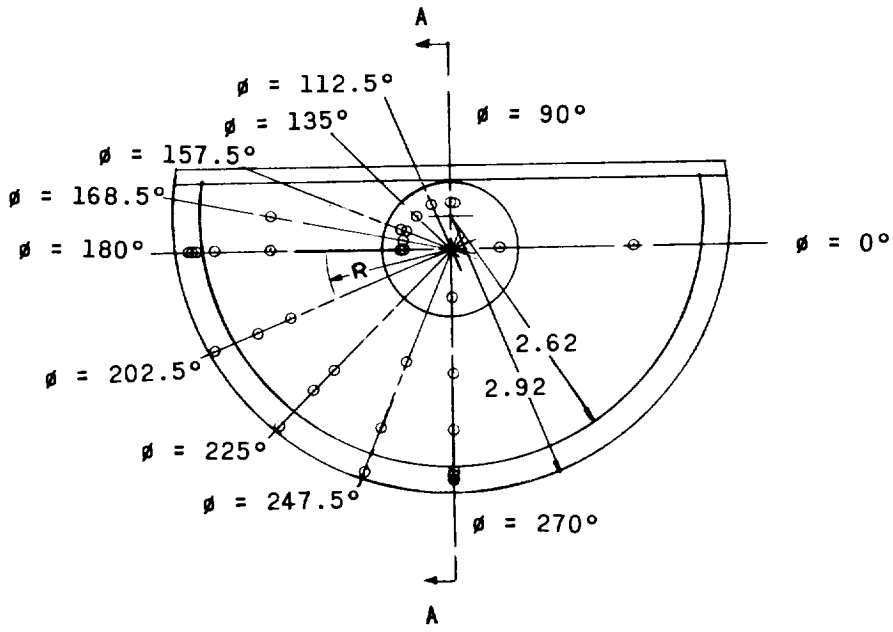

Orifice Locations

Orifice	ø, deg	R, in.
1	0	0.50
2	0	1.90
3	90	.50
4	90	.50
5	112.5	.50
6	135	.50
7	157.5	.56
8	157.5	.63
9	168.5	.50
10	168.5	1.90
11	180	.50
12	180	.50
13	180	1.90
14	180	2.45
15	180	2.70
16	180	2.75
17	180	2.80
18	202.5	1.80
19	202.5	2.20
20	202.5	2.70
21	225	1.77
22	225	2.07
23	225	2.60
24	247.5	1.25
25	247.5	2.00
26	247.5	2.50
27	270	.50
28	270	1.30
29	270	1.90
30	270	2.30
31	270	2.37
32	270	2.45

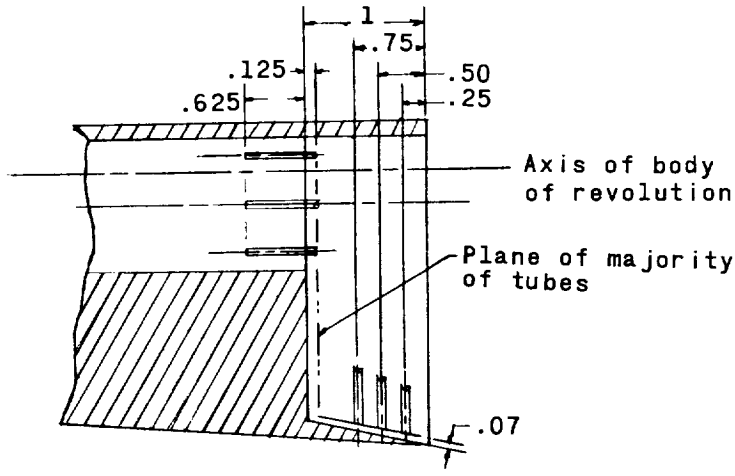

Figure 5.- Details of base of body B_3. Dimensions are in inches unless otherwise noted.

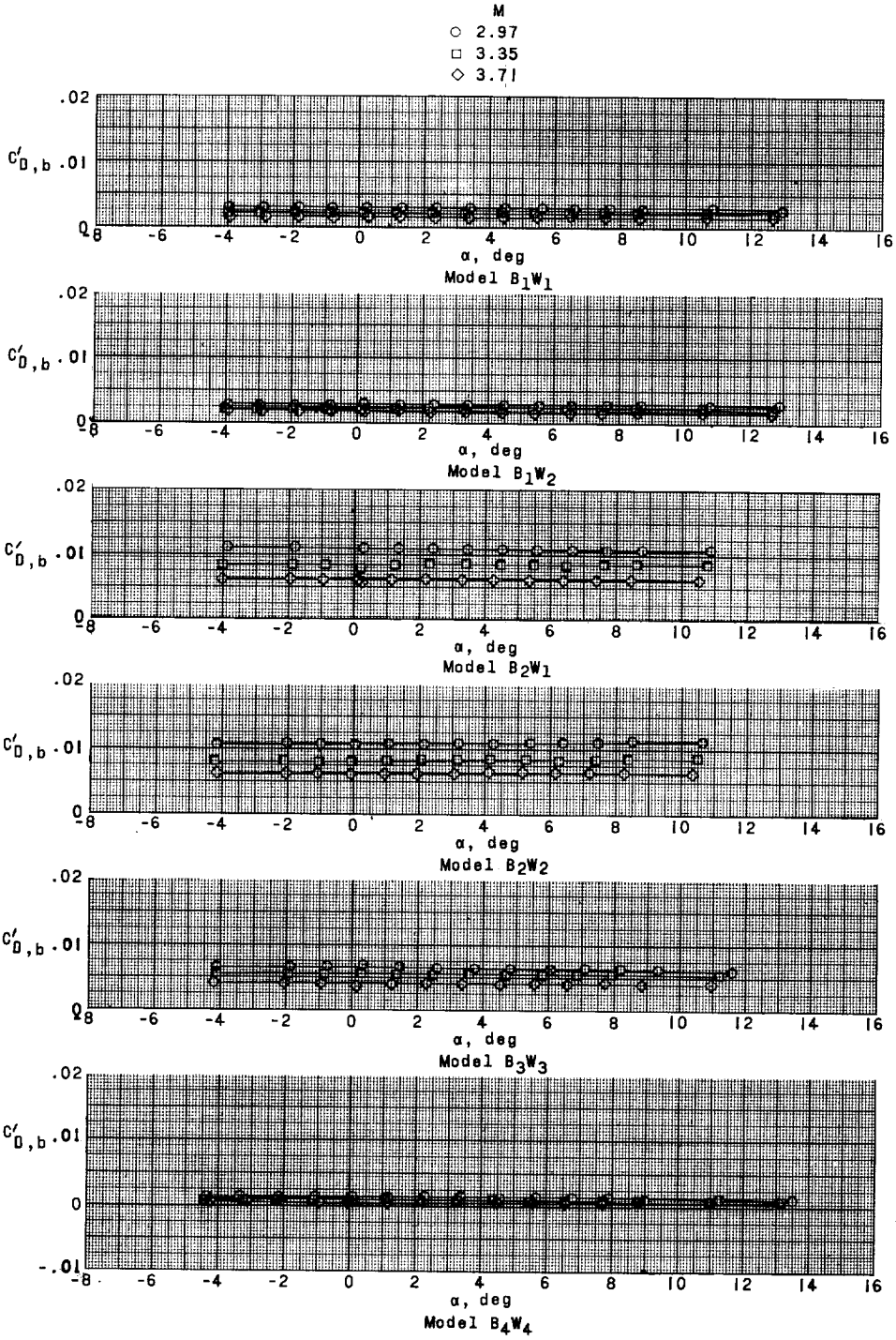

Figure 6.- Variation of base drag coefficient with angle of attack for the various model configurations.

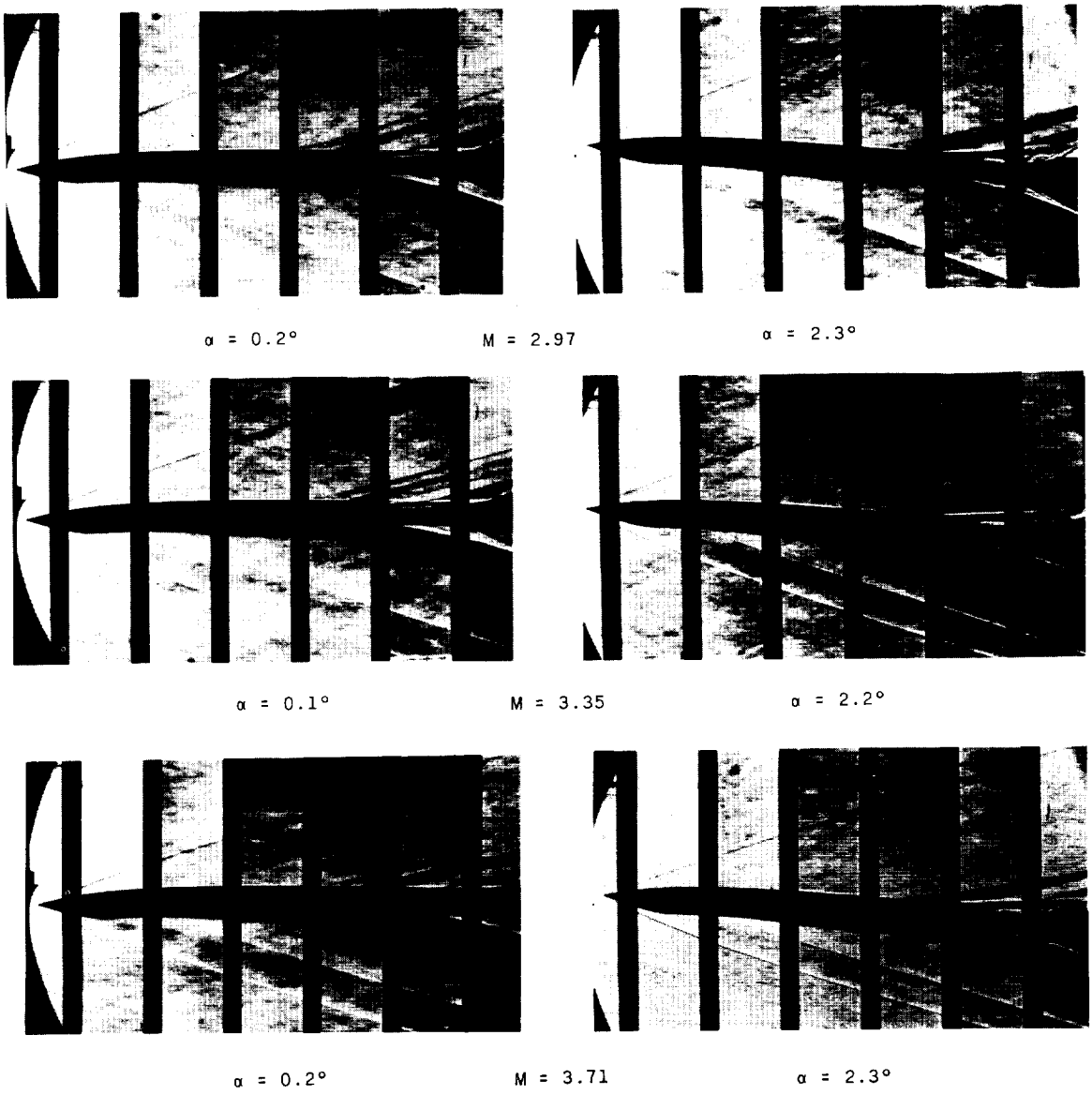

(a) Model B_1W_1. L-58-111a

Figure 7.- Typical schlieren photographs of the various models.

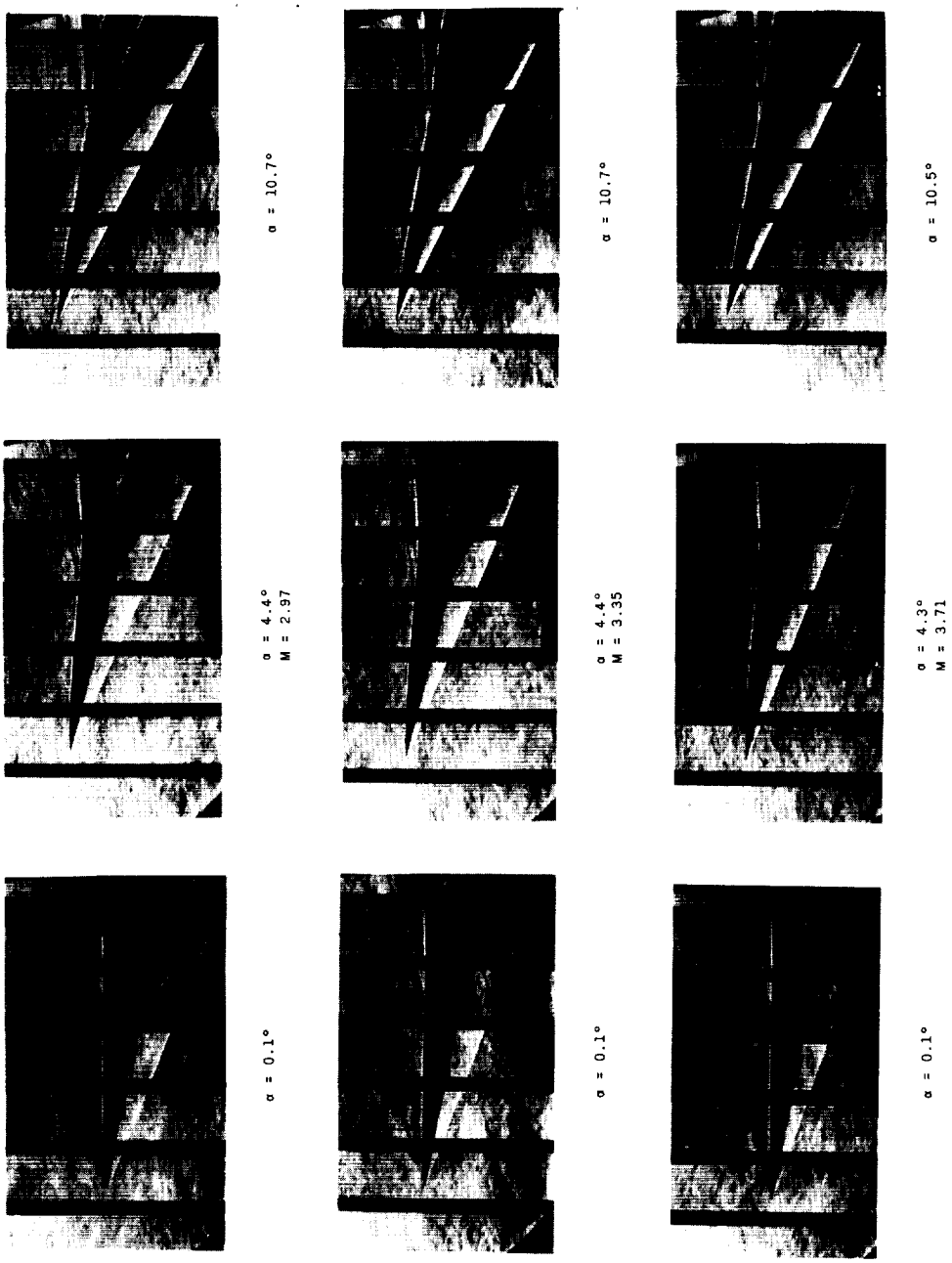

(b) Model B_1W_2.

L-58-112a

Figure 7.- Continued.

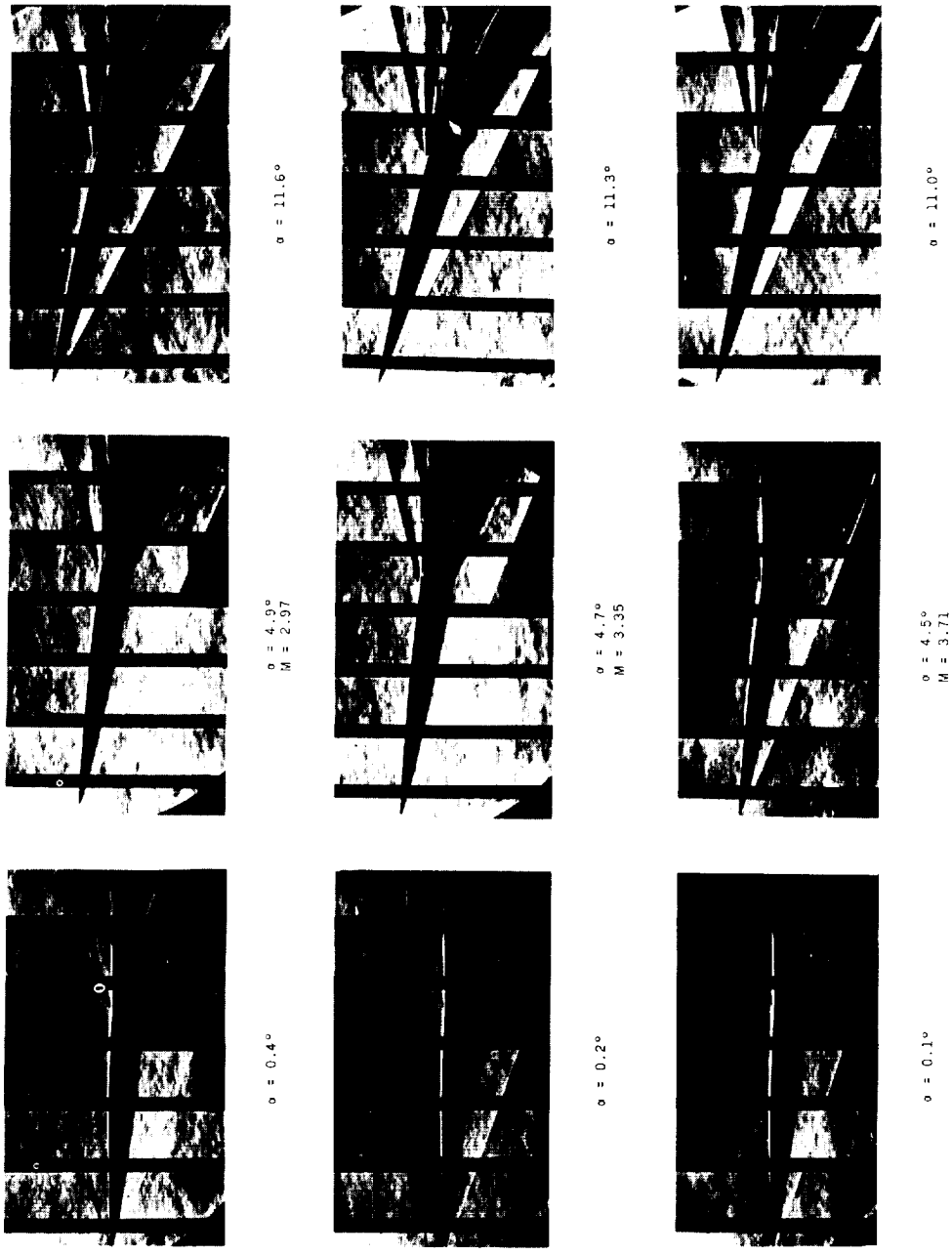

(c) Model B_3W_3. L-58-113a

Figure 7.- Continued.

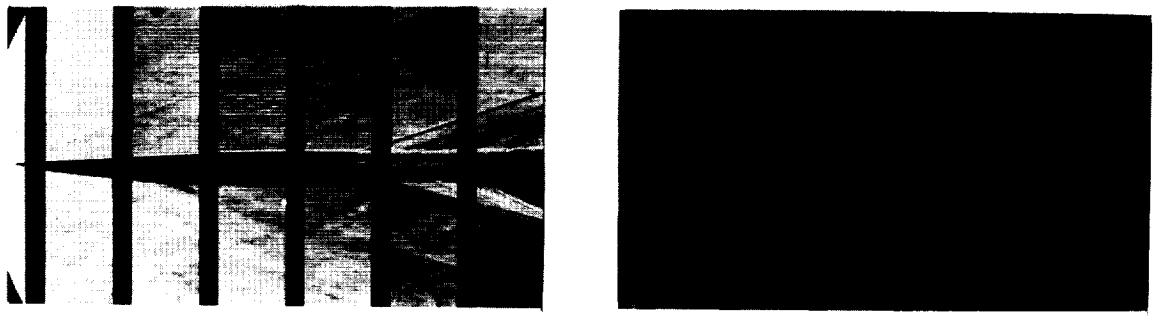

α = 0.1° M = 2.97 α = 2.2°

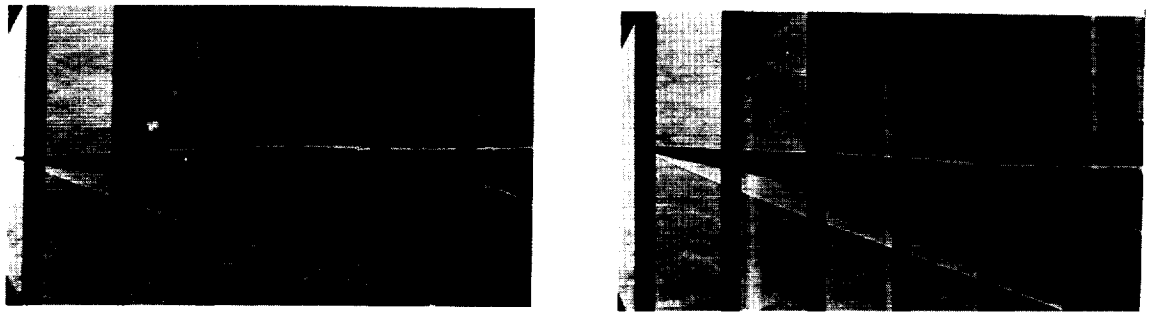

α = -0.1° M = 3.35 α = 2.1°

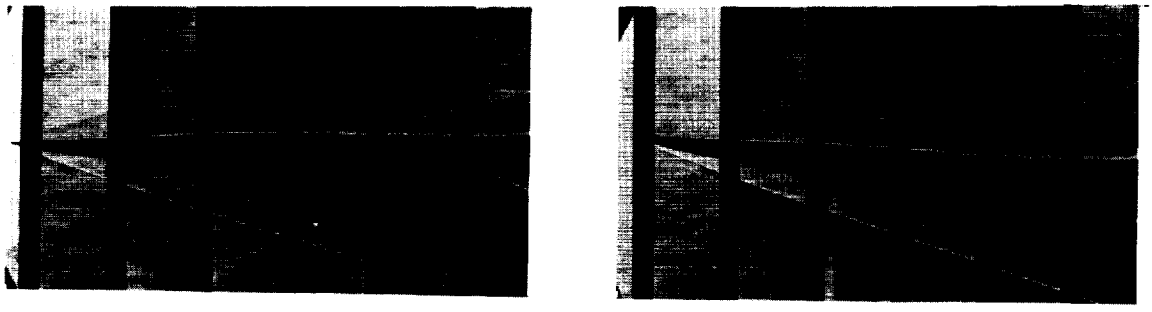

α = 0.0° M = 3.71 α = 2.3°

(d) Model B_4W_4. L-58-114a

Figure 7.- Concluded.

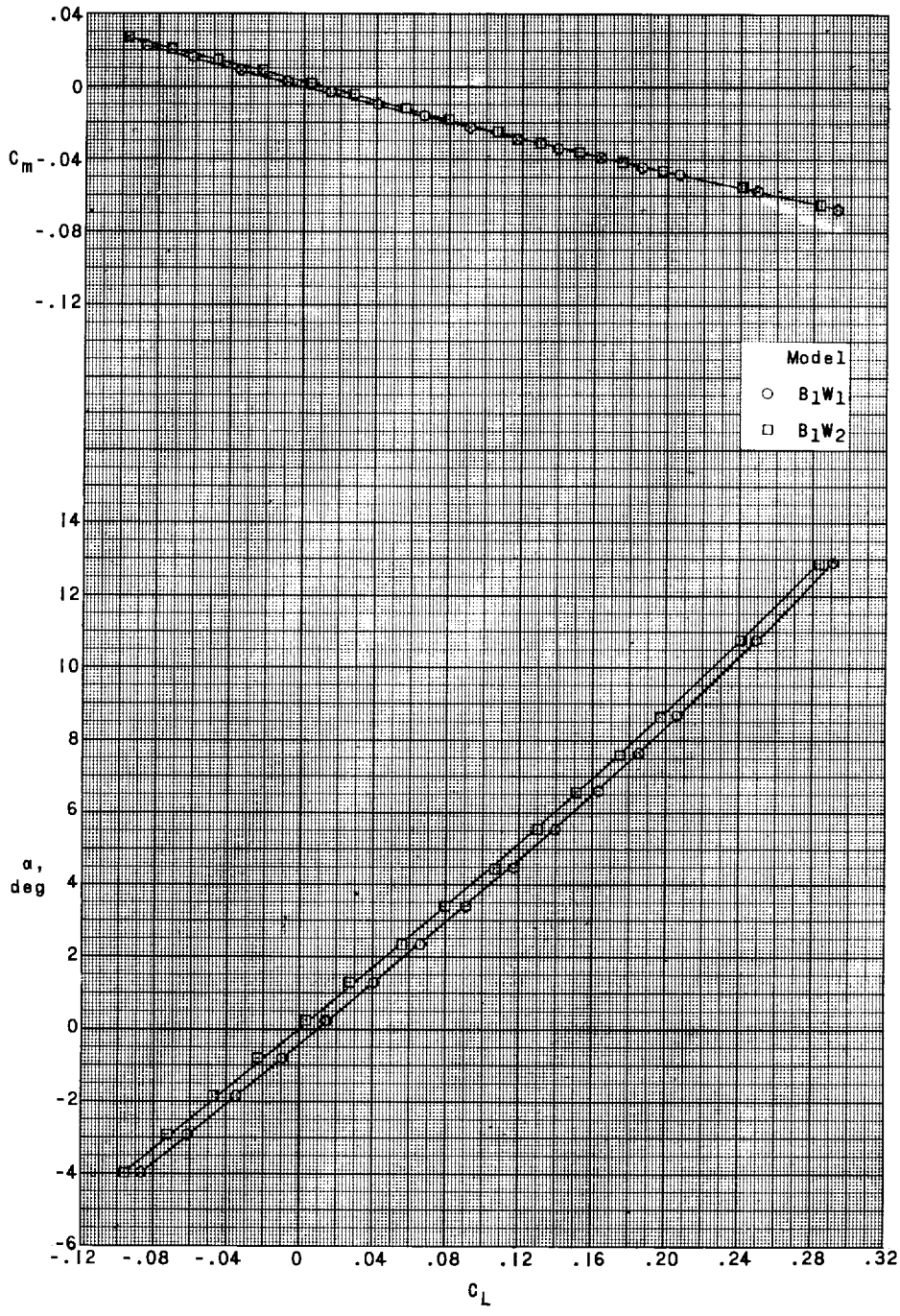

(a) M = 2.97.

Figure 8.- Longitudinal characteristics of B_1W_1 and B_1W_2.

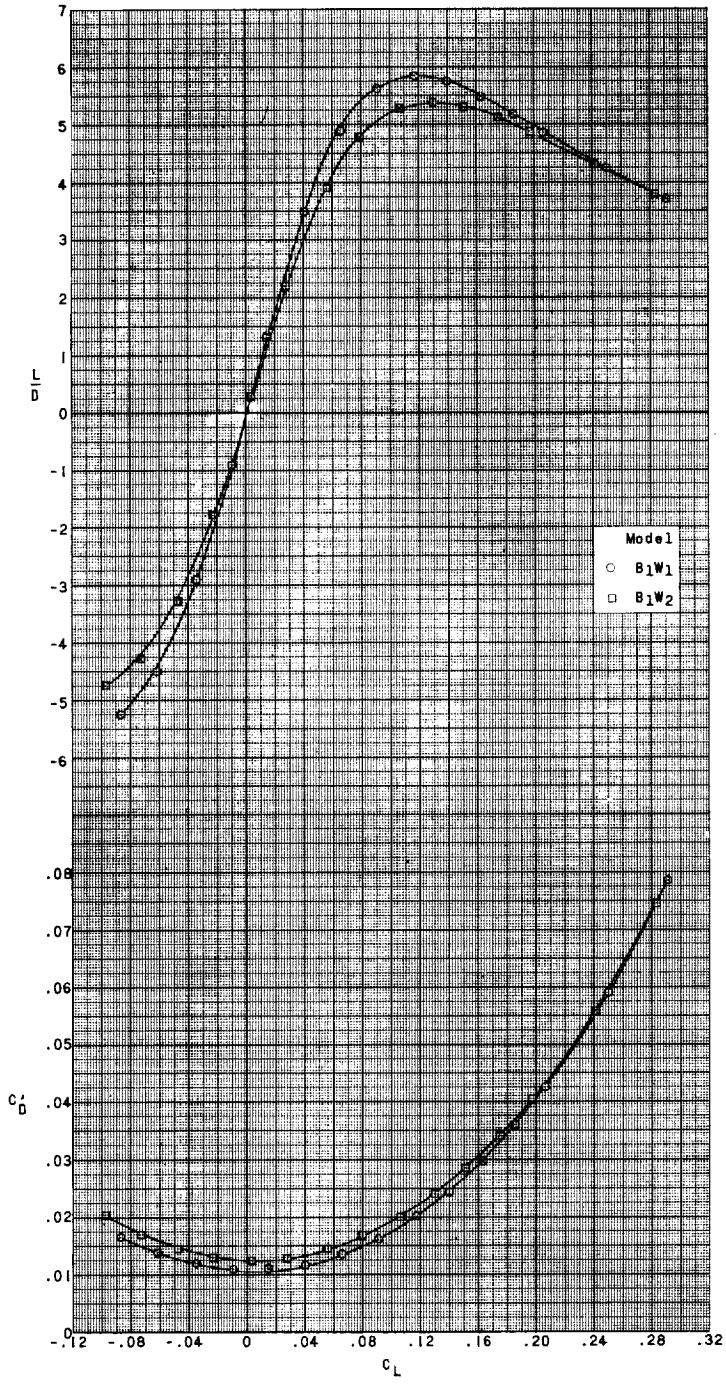

(a) Concluded.

Figure 8.- Continued.

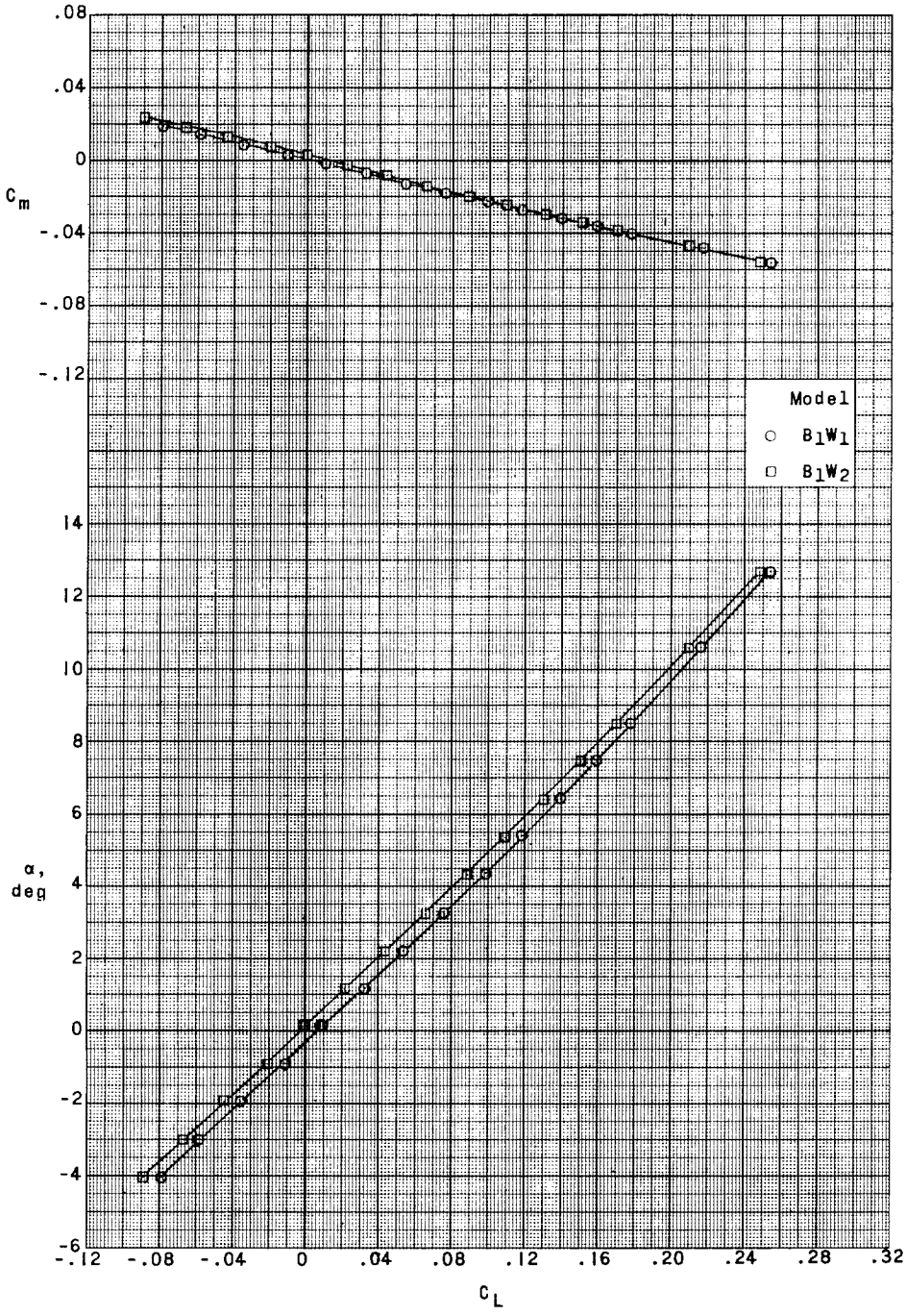

(b) M = 3.35.

Figure 8.- Continued.

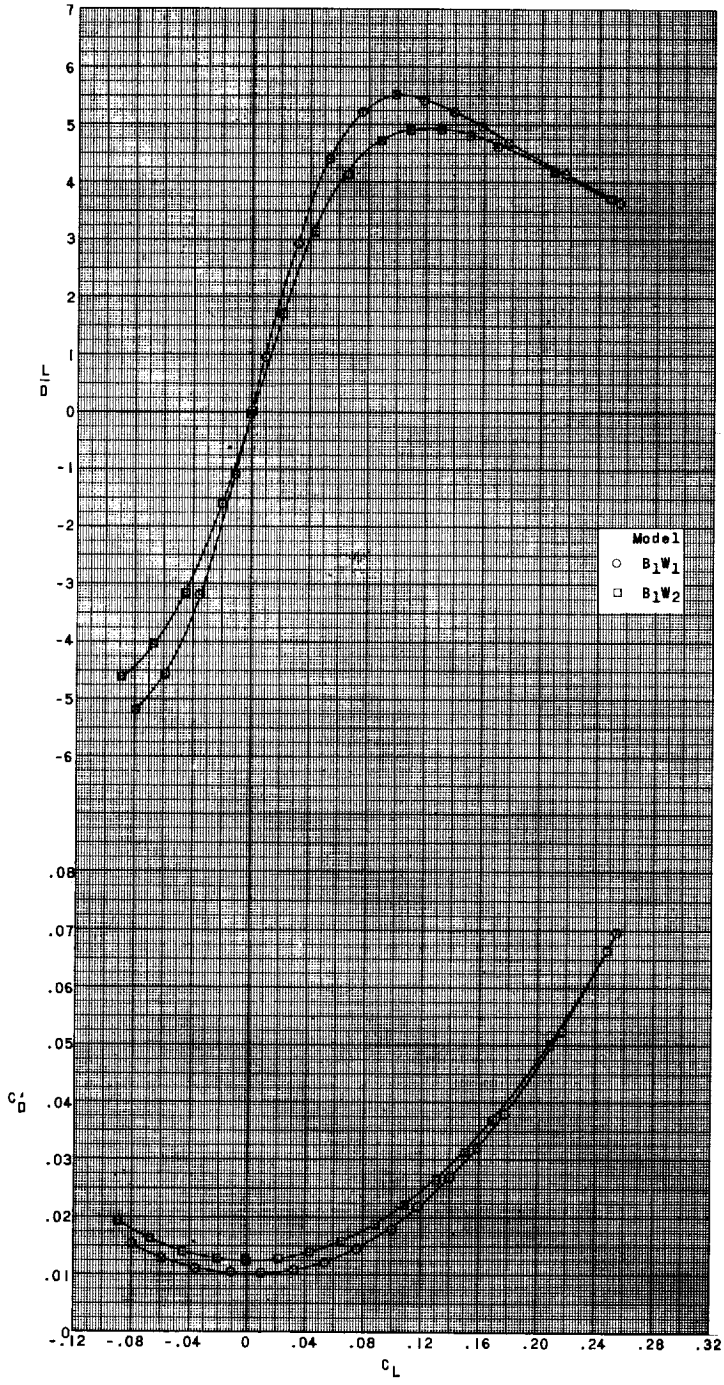

(b) Concluded.

Figure 8.- Continued.

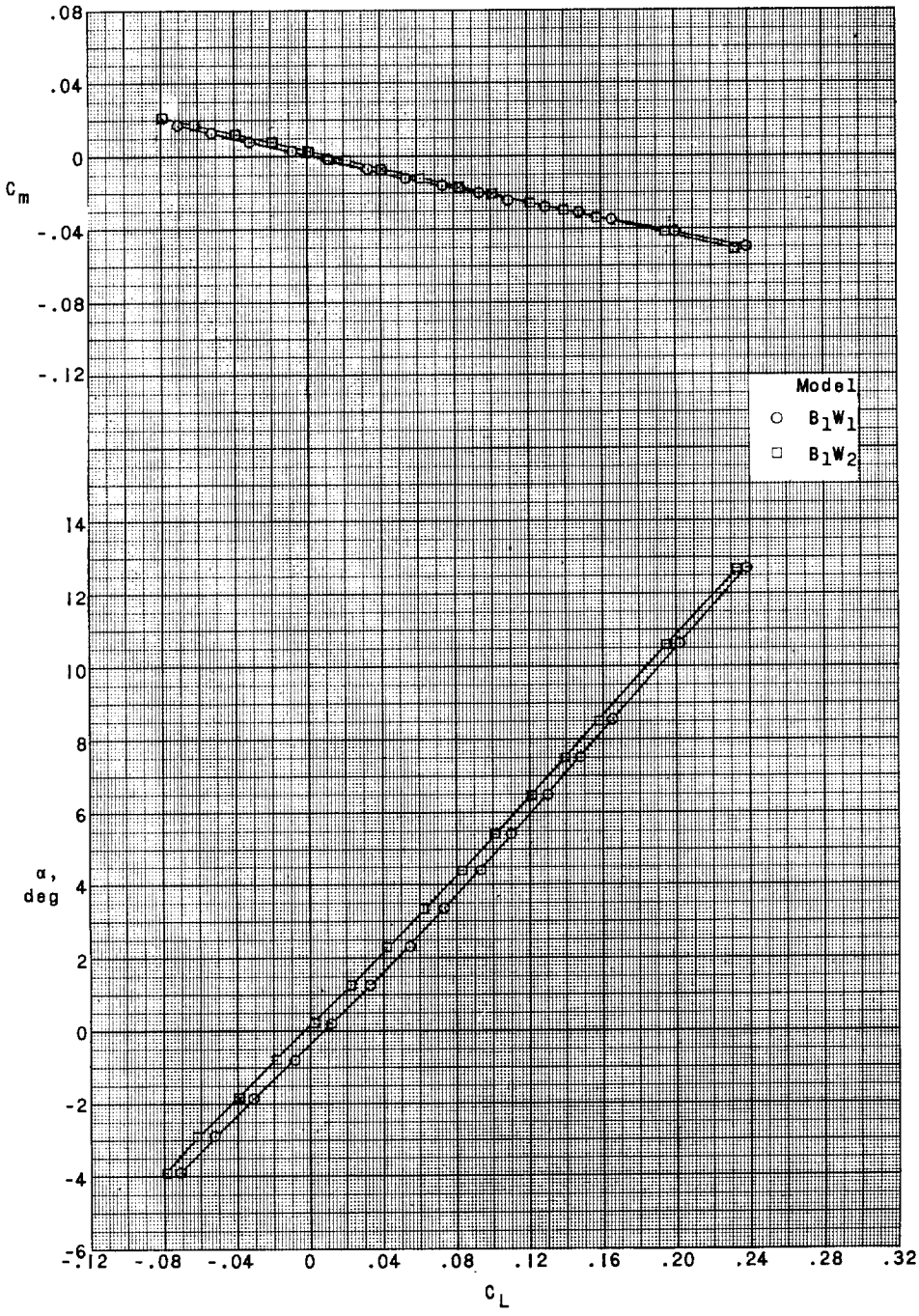

(c) M = 3.71.

Figure 8.- Continued.

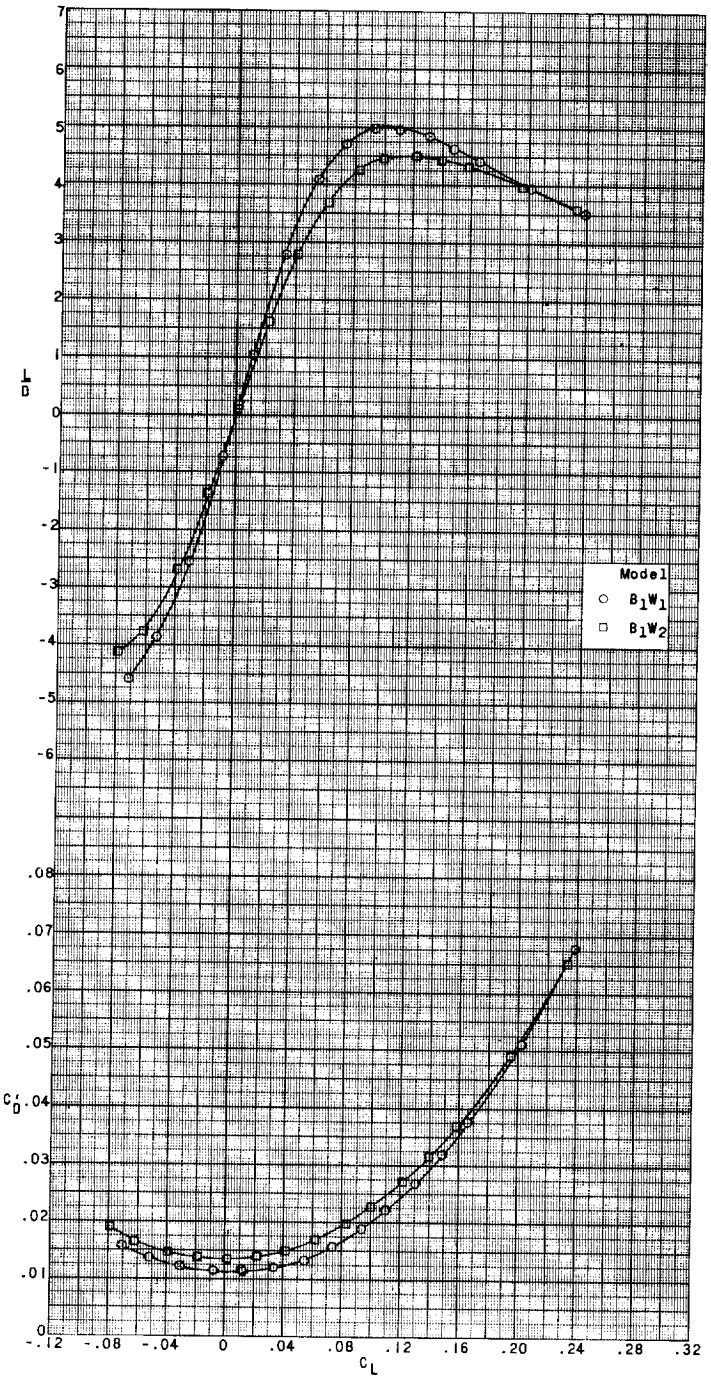

(c) Concluded.

Figure 8.- Concluded.

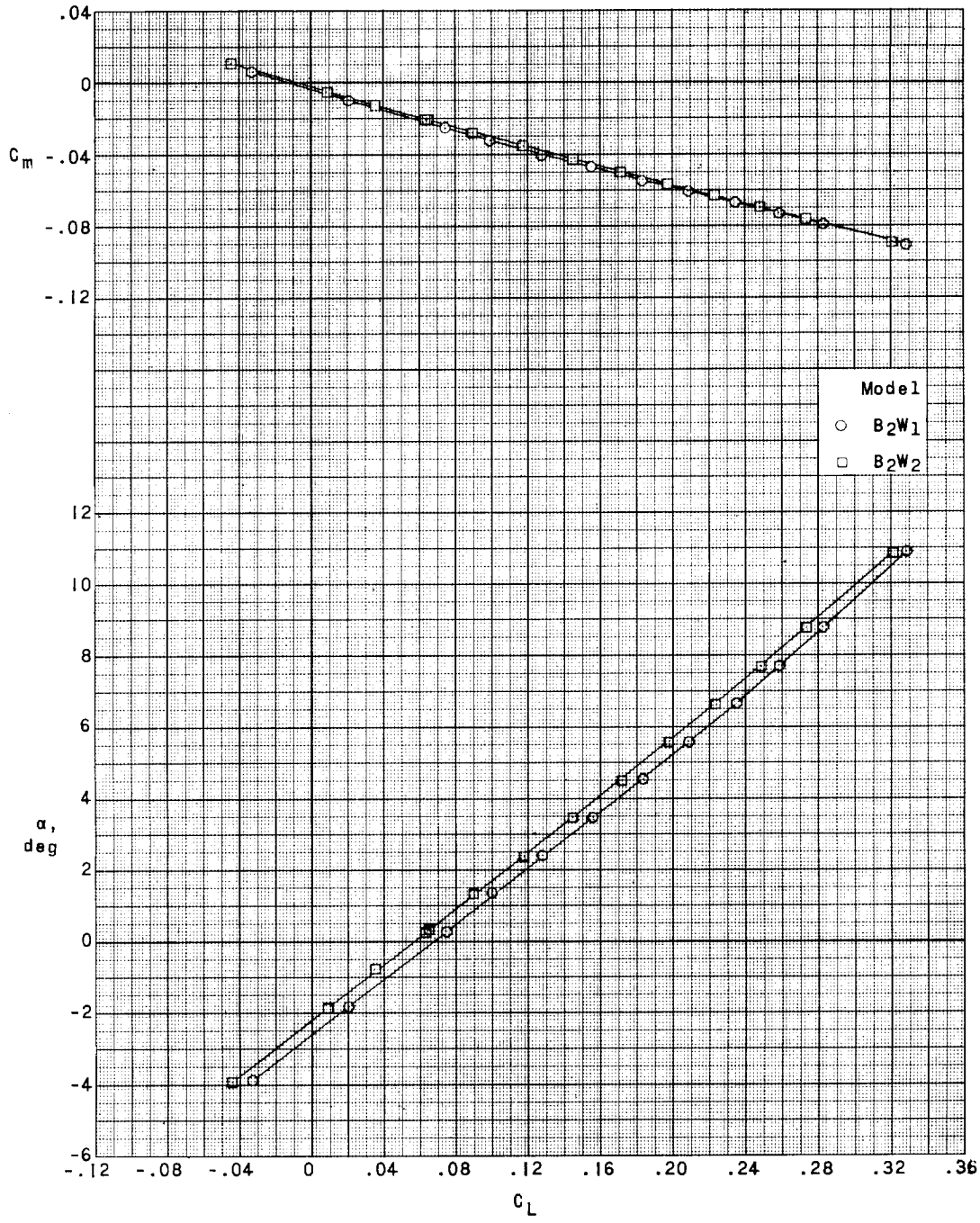

(a) M = 2.97.

Figure 9.- Longitudinal characteristics of B_2W_1 and B_2W_2.

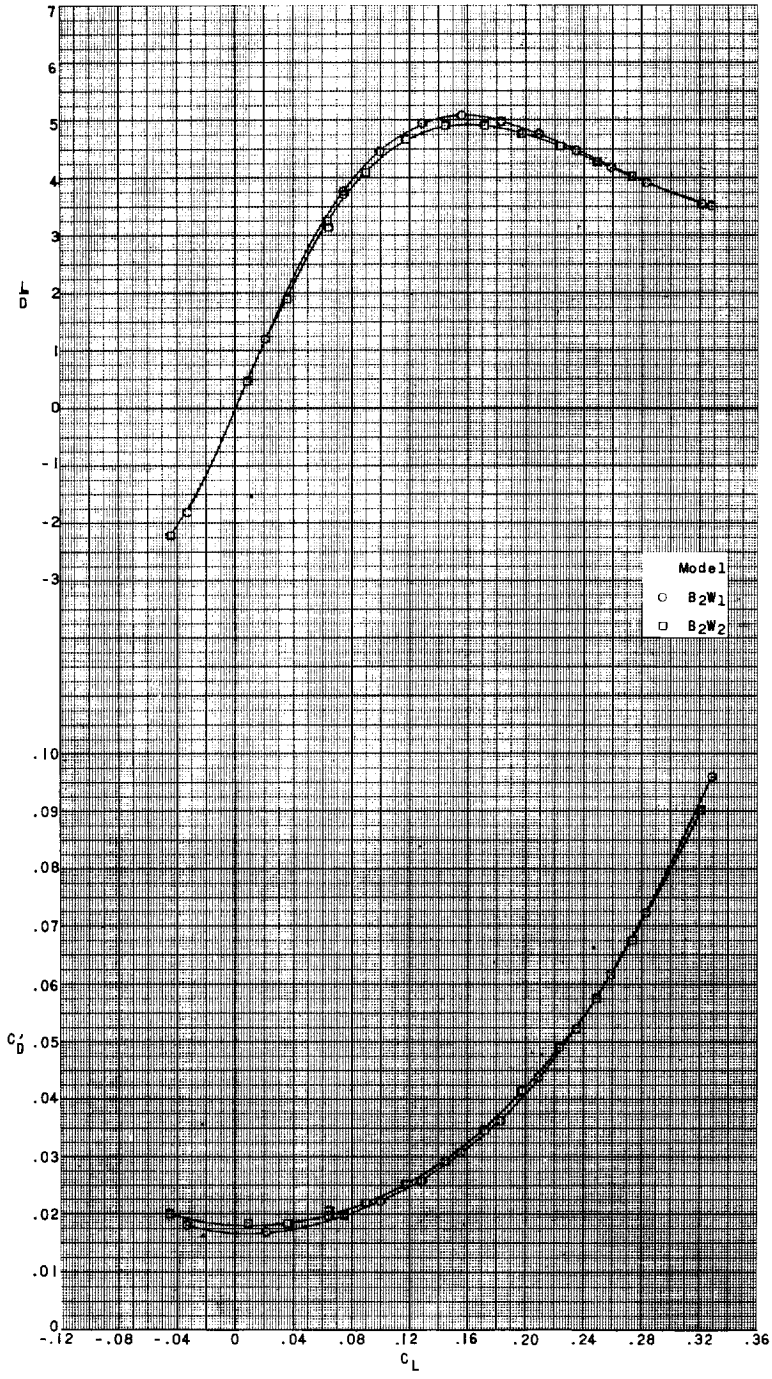

(a) Concluded.

Figure 9.- Continued.

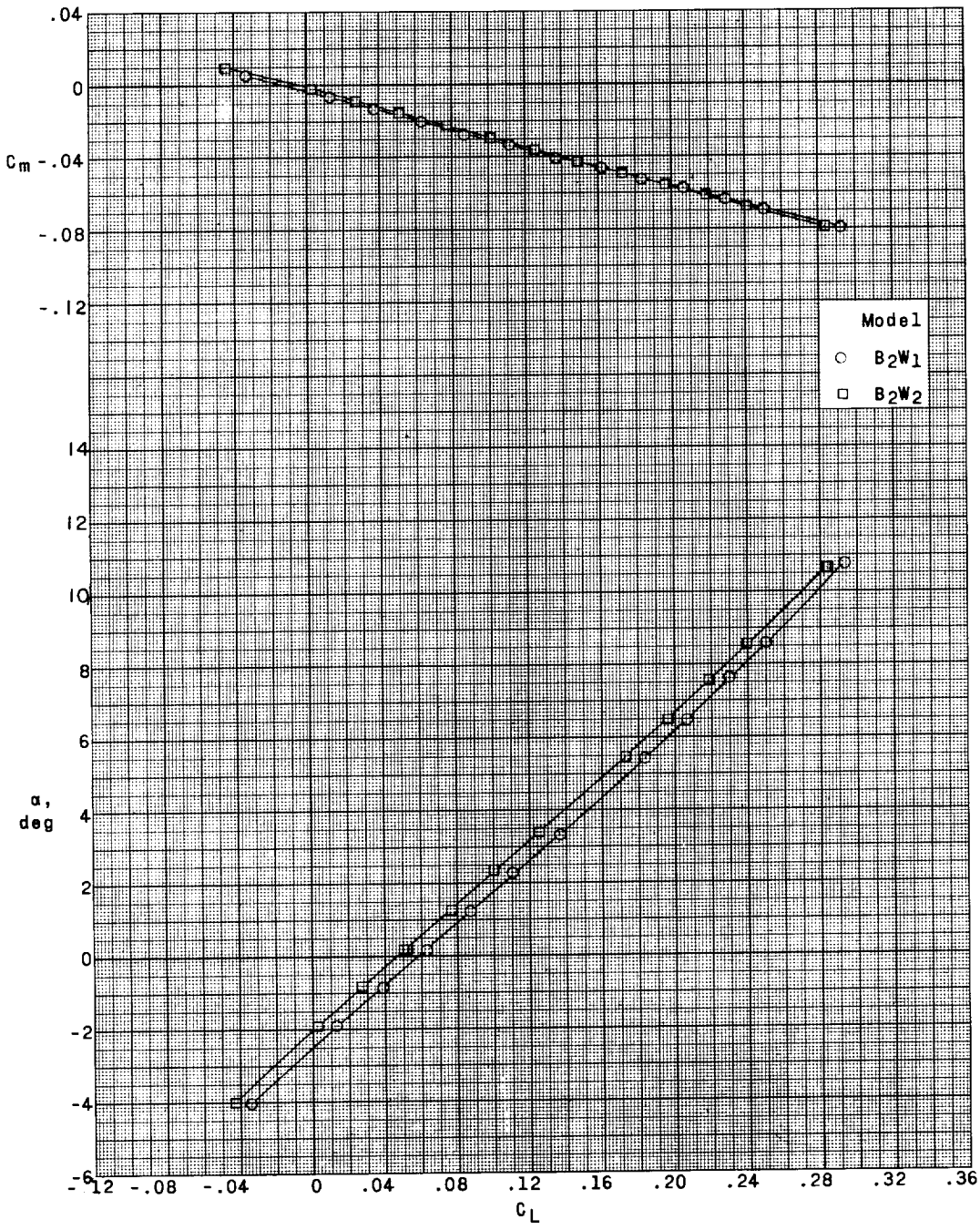

(b) M = 3.35.

Figure 9.- Continued.

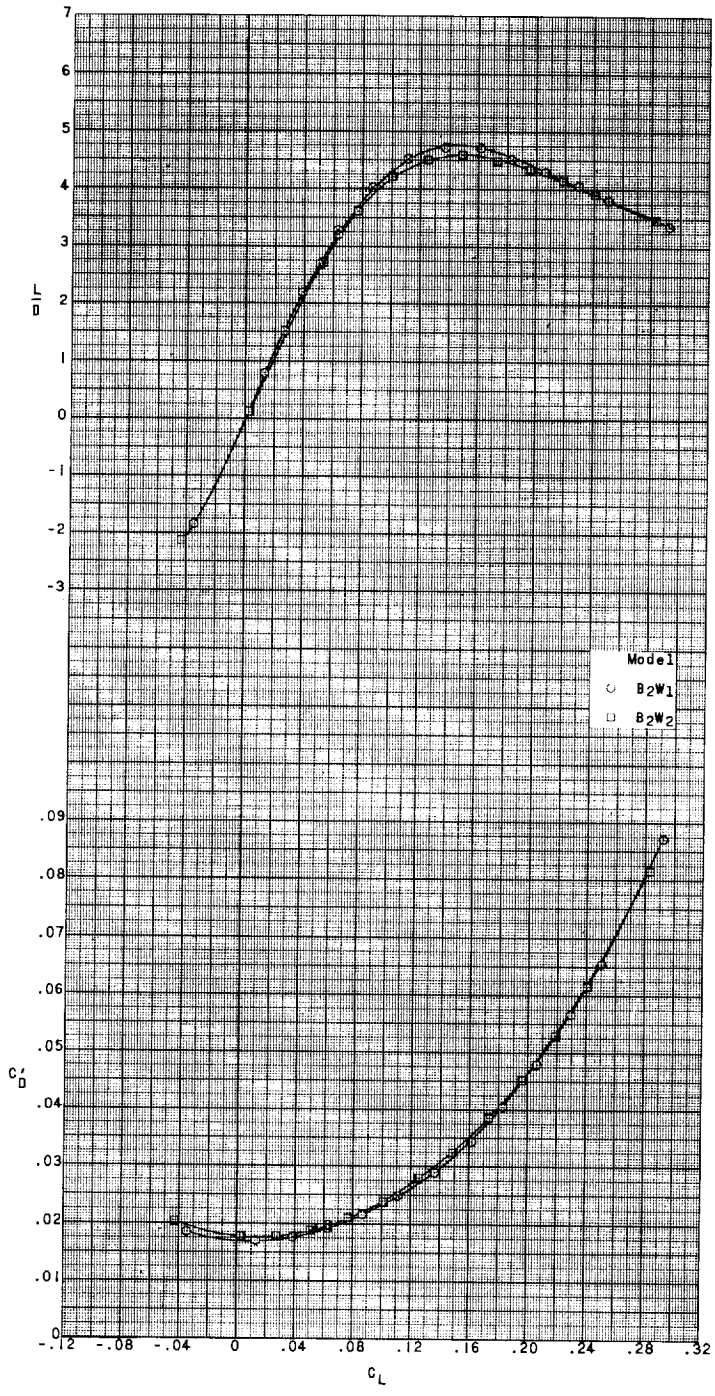

(b) Concluded.

Figure 9.- Continued.

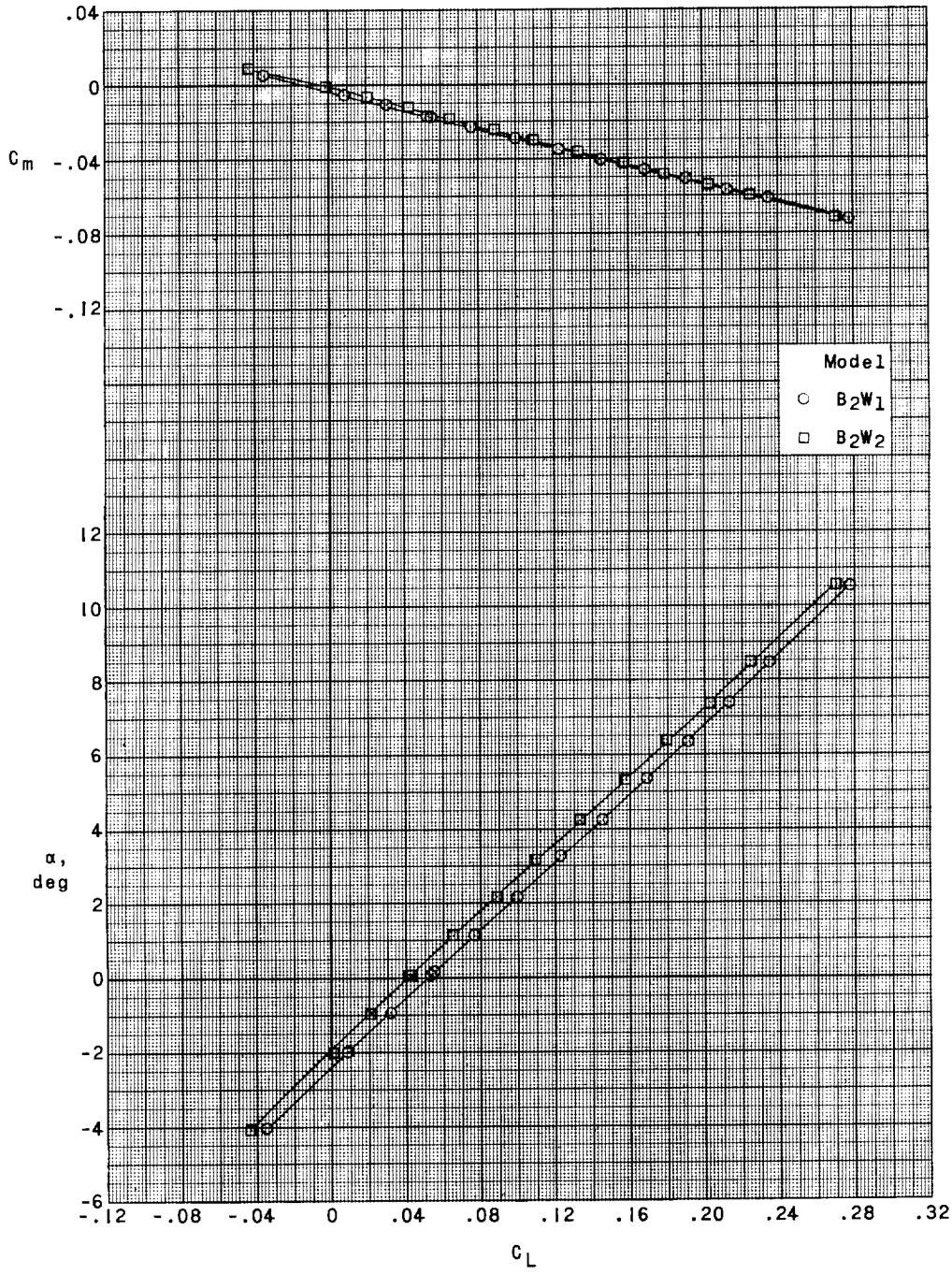

(c) M = 3.71.

Figure 9.- Continued.

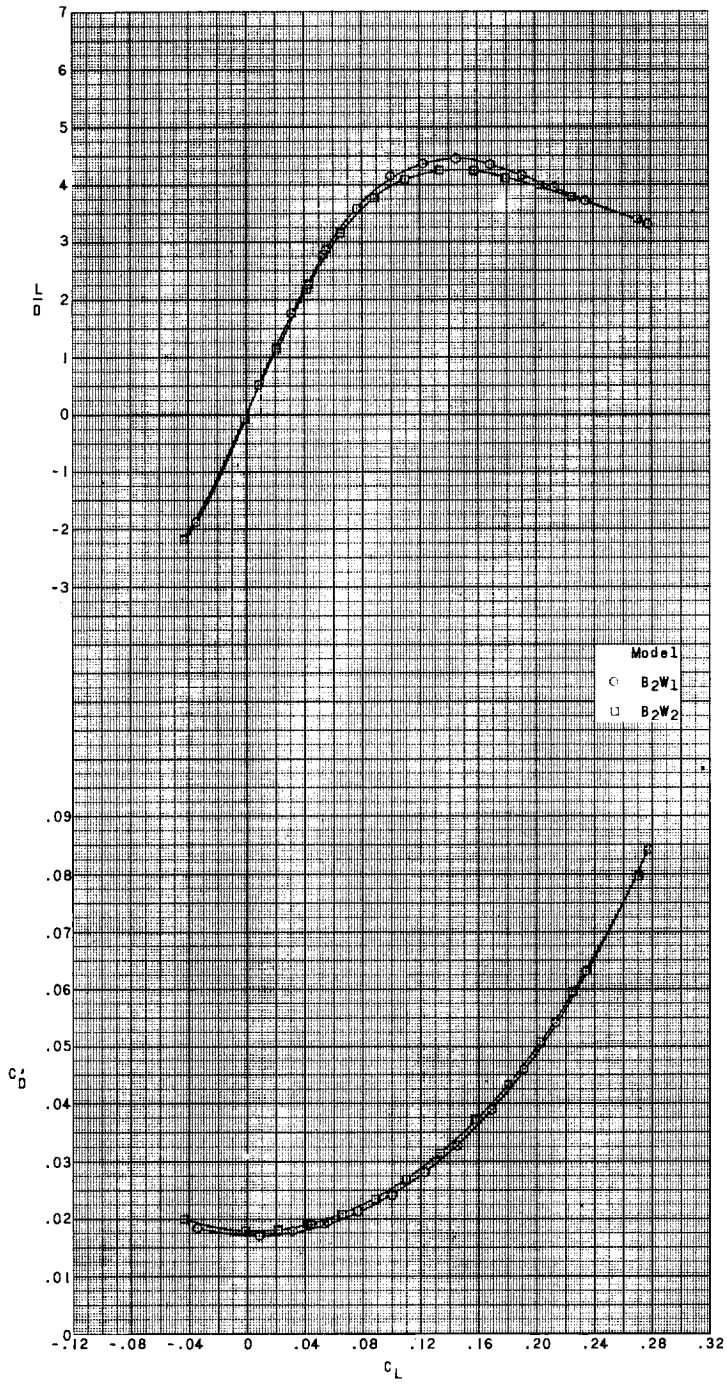

(c) Concluded.

Figure 9.- Concluded.

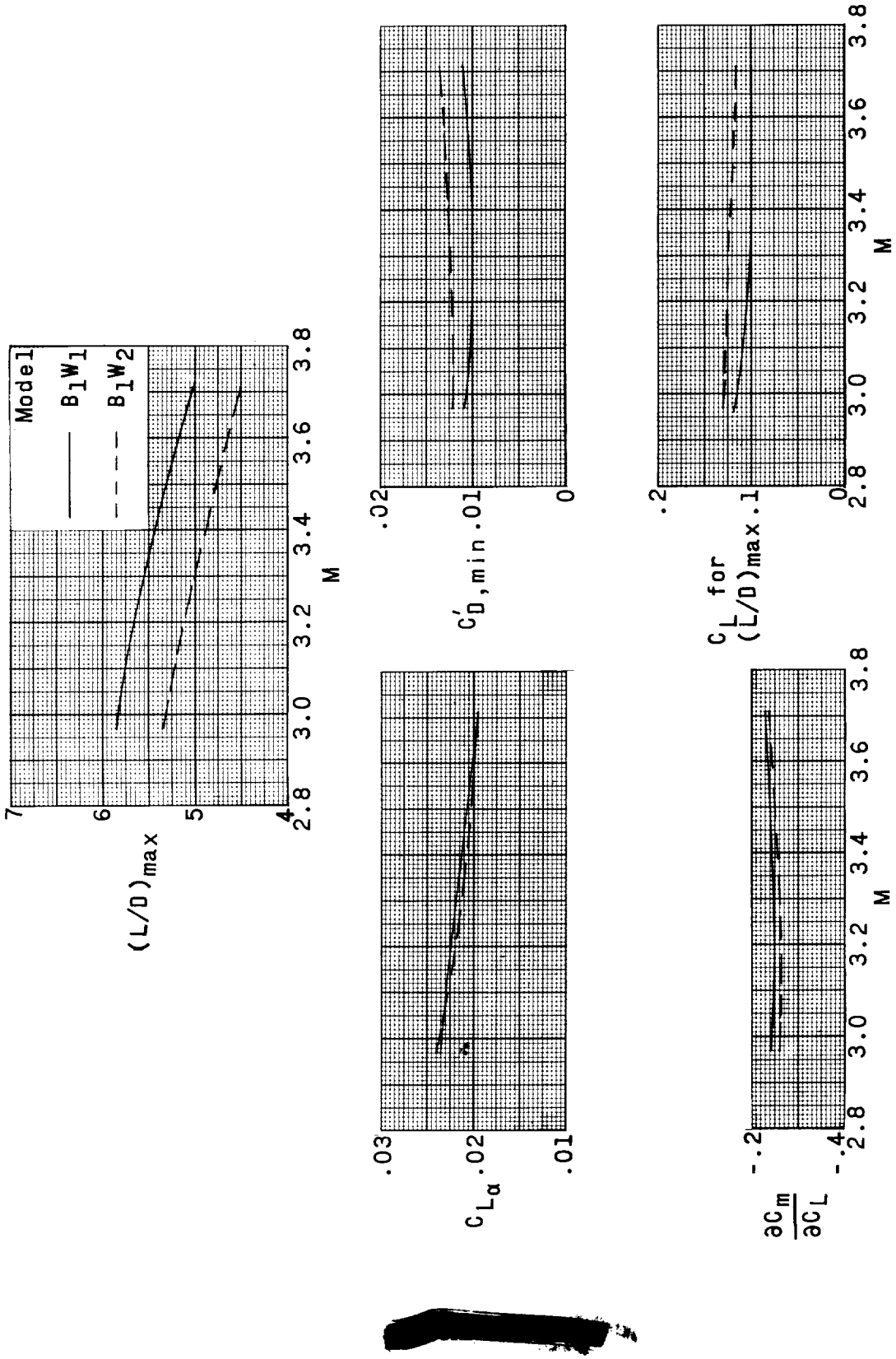

(a) With body B_1.

Figure 10.- Summary of longitudinal characteristics for the arrow-wing models.

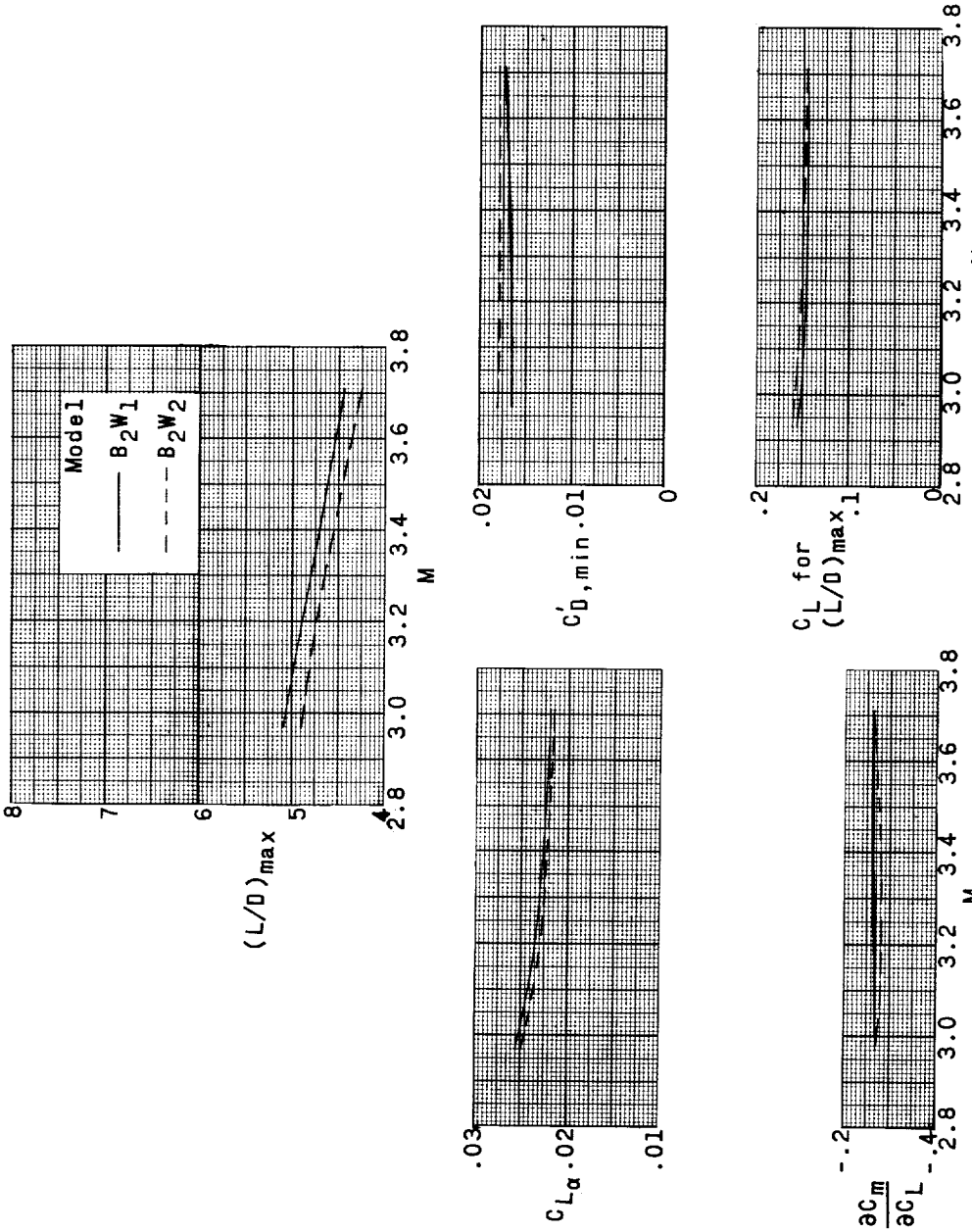

(b) With body B_2.

Figure 10.- Concluded.

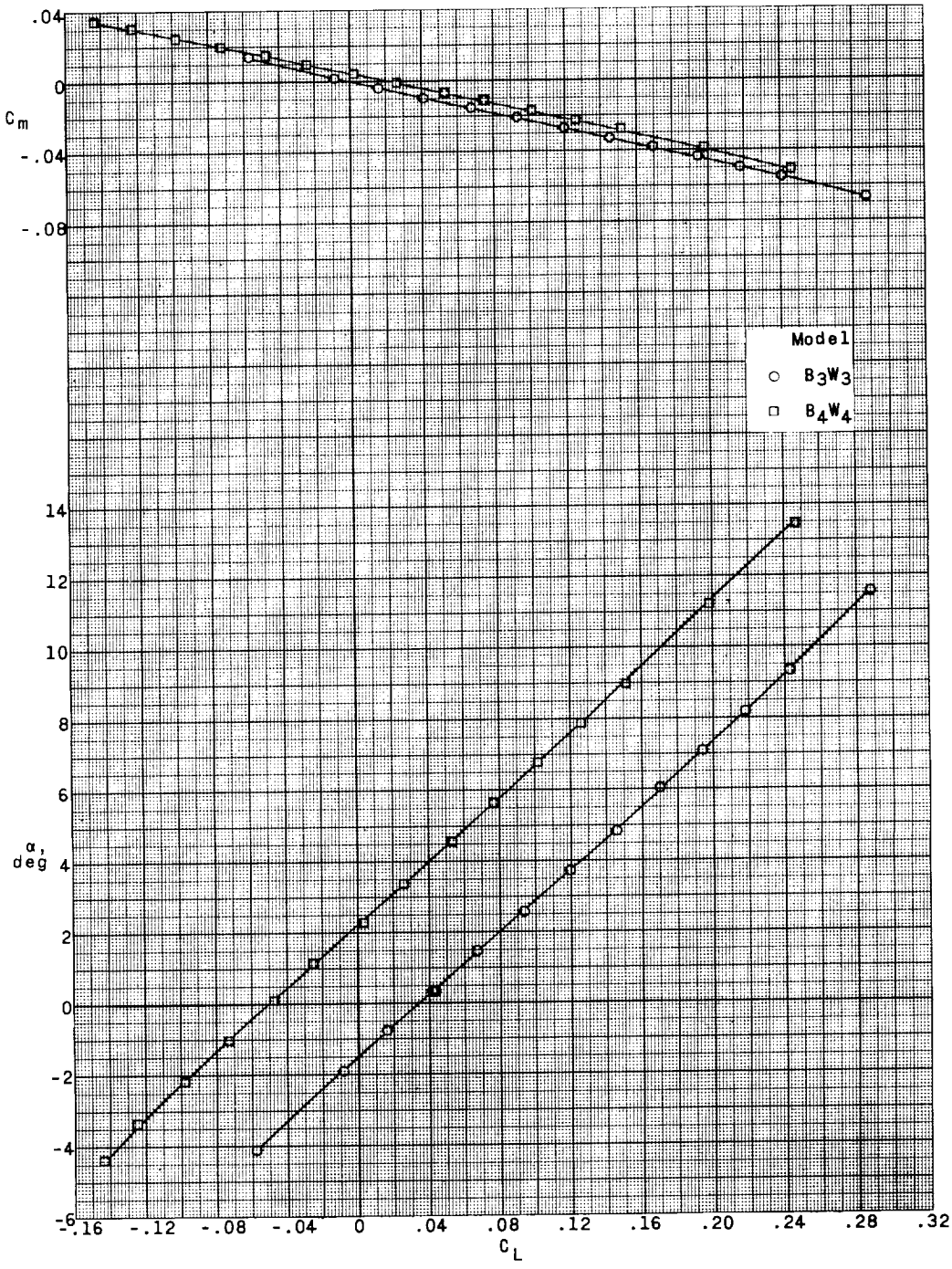

(a) M = 2.97.

Figure 11.- Longitudinal characteristics of B_3W_3 and B_4W_4.

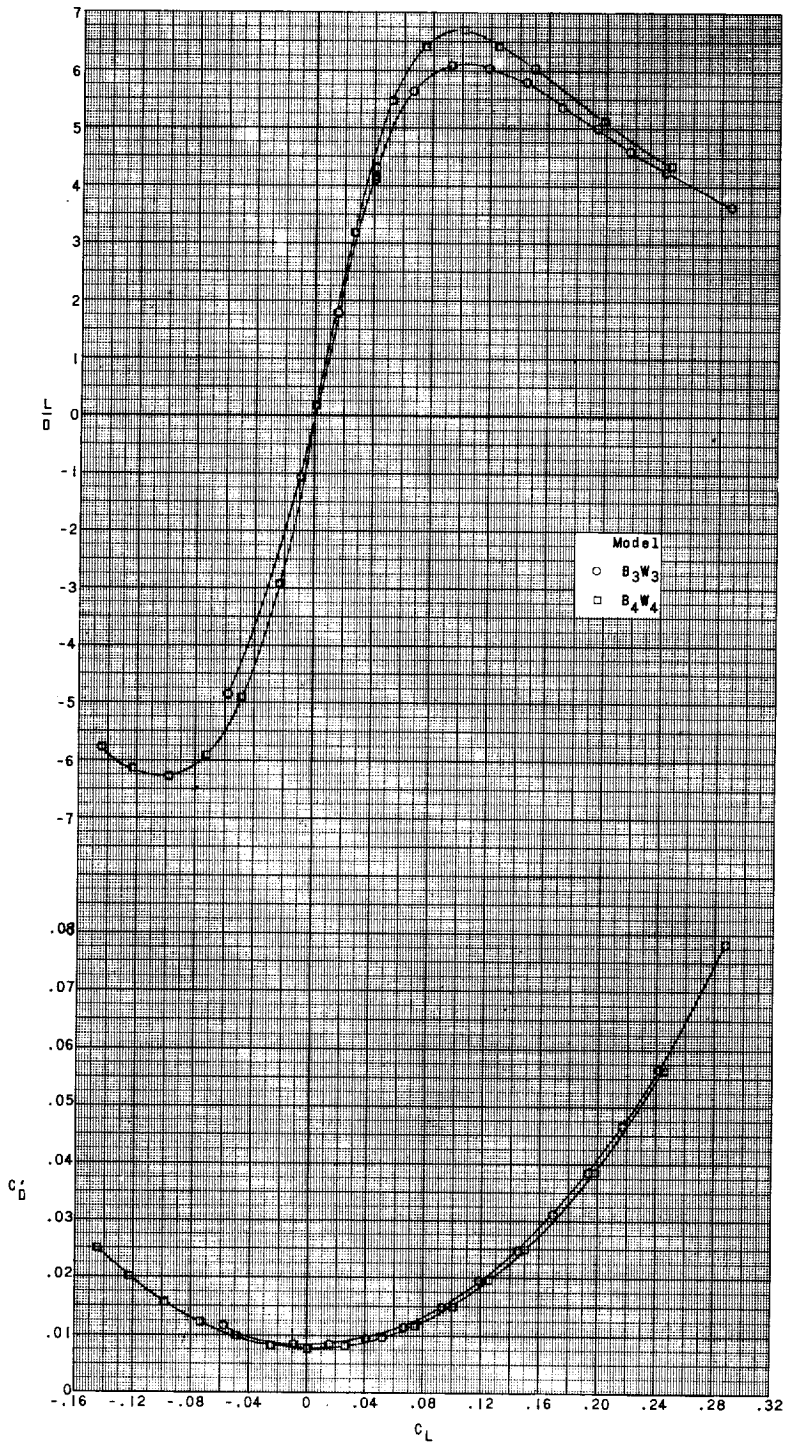

(a) Concluded.

Figure 11.- Continued.

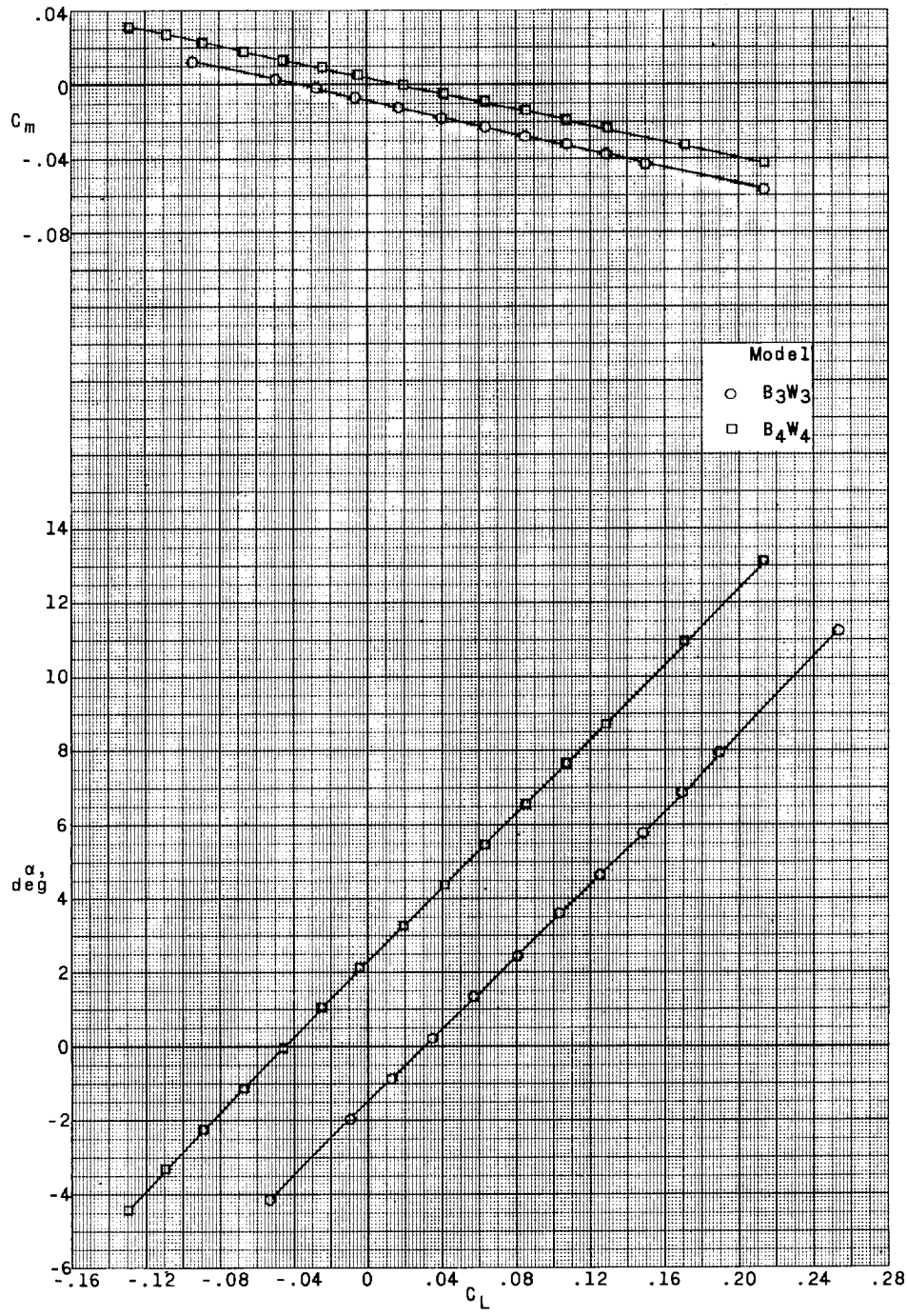

(b) M = 3.35.

Figure 11.- Continued.

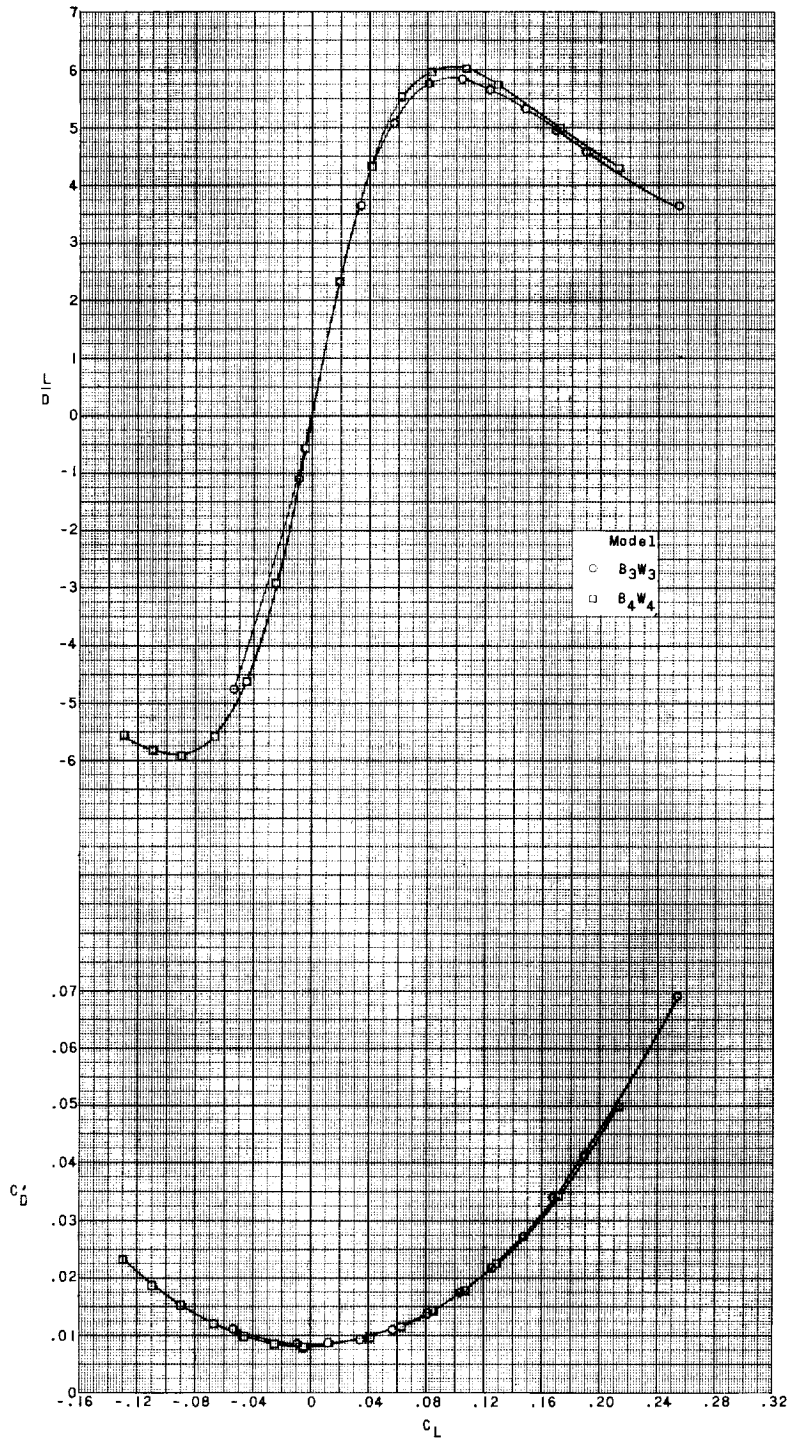

(b) Concluded.

Figure 11.- Continued.

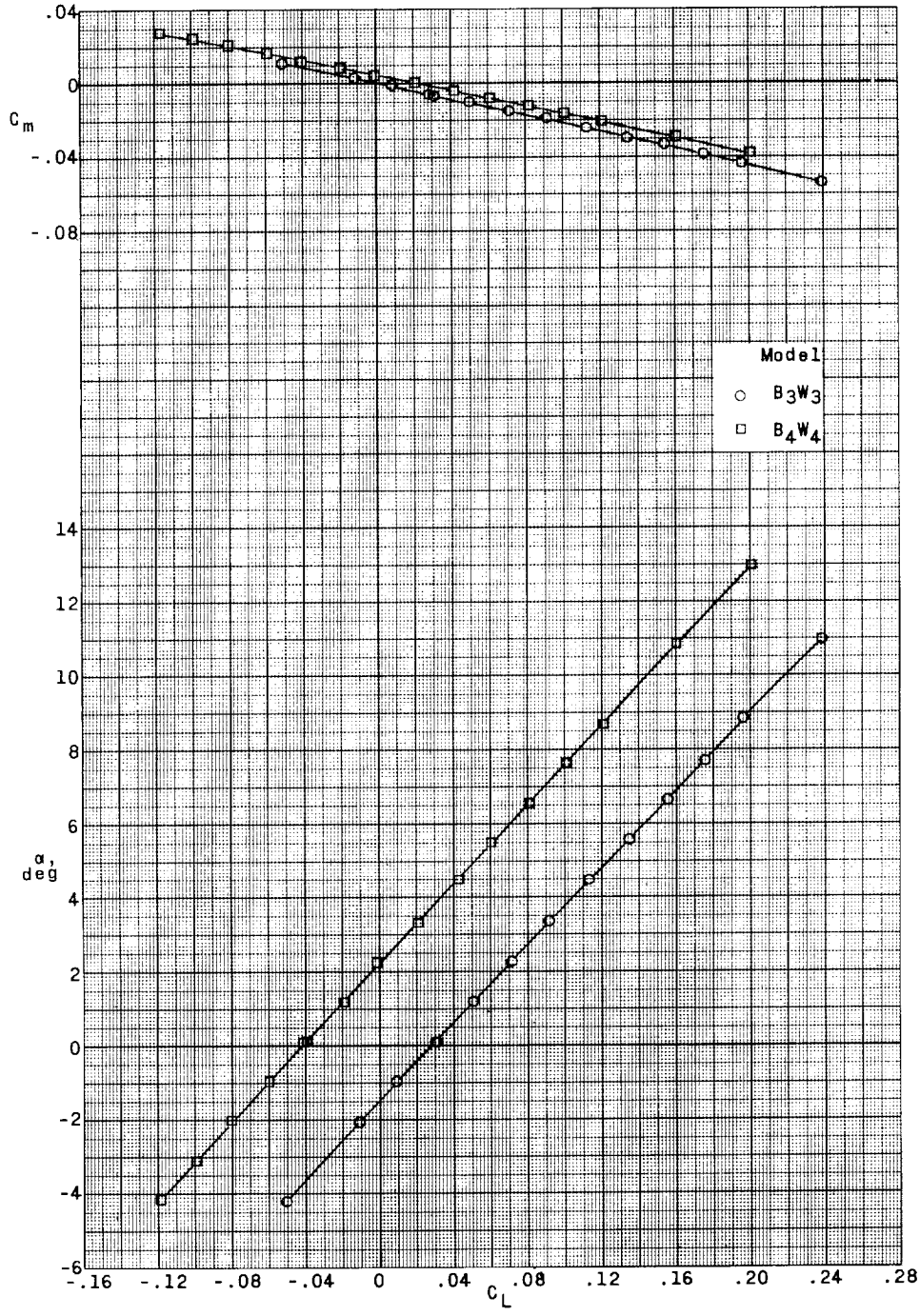

(c) M = 3.71.

Figure 11.- Continued.

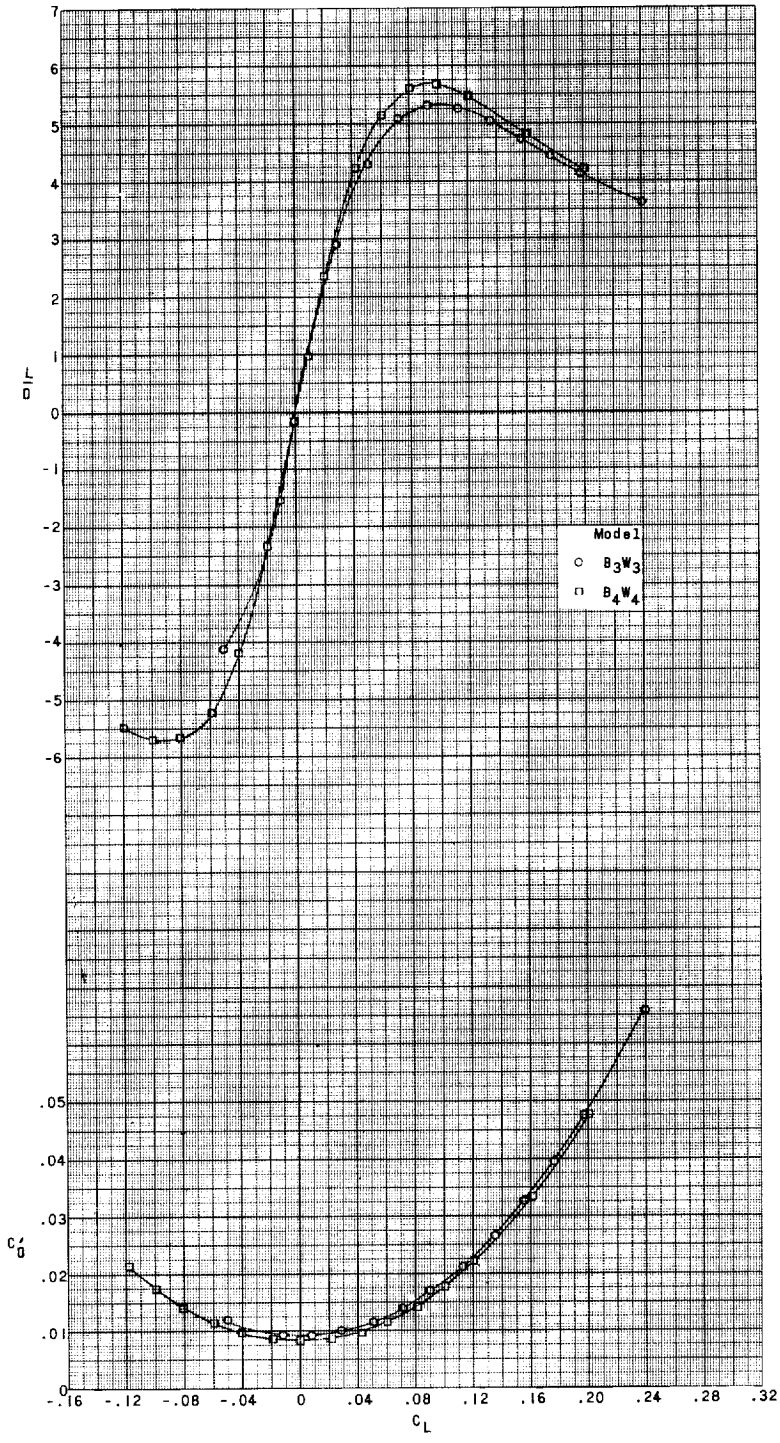

(c) Concluded.

Figure 11.- Concluded.

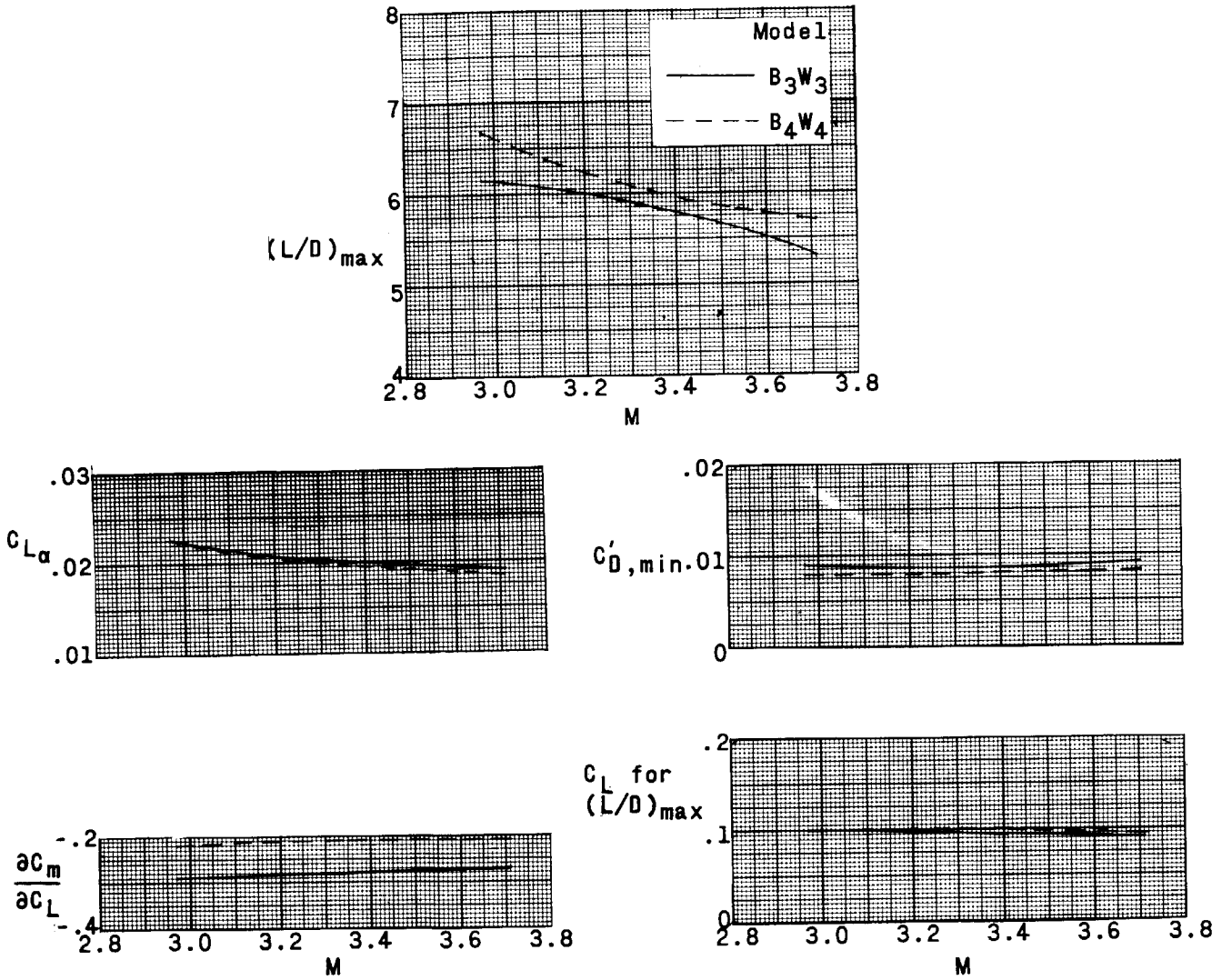

Figure 12.- Summary of longitudinal characteristics for the modified-diamond-wing models.

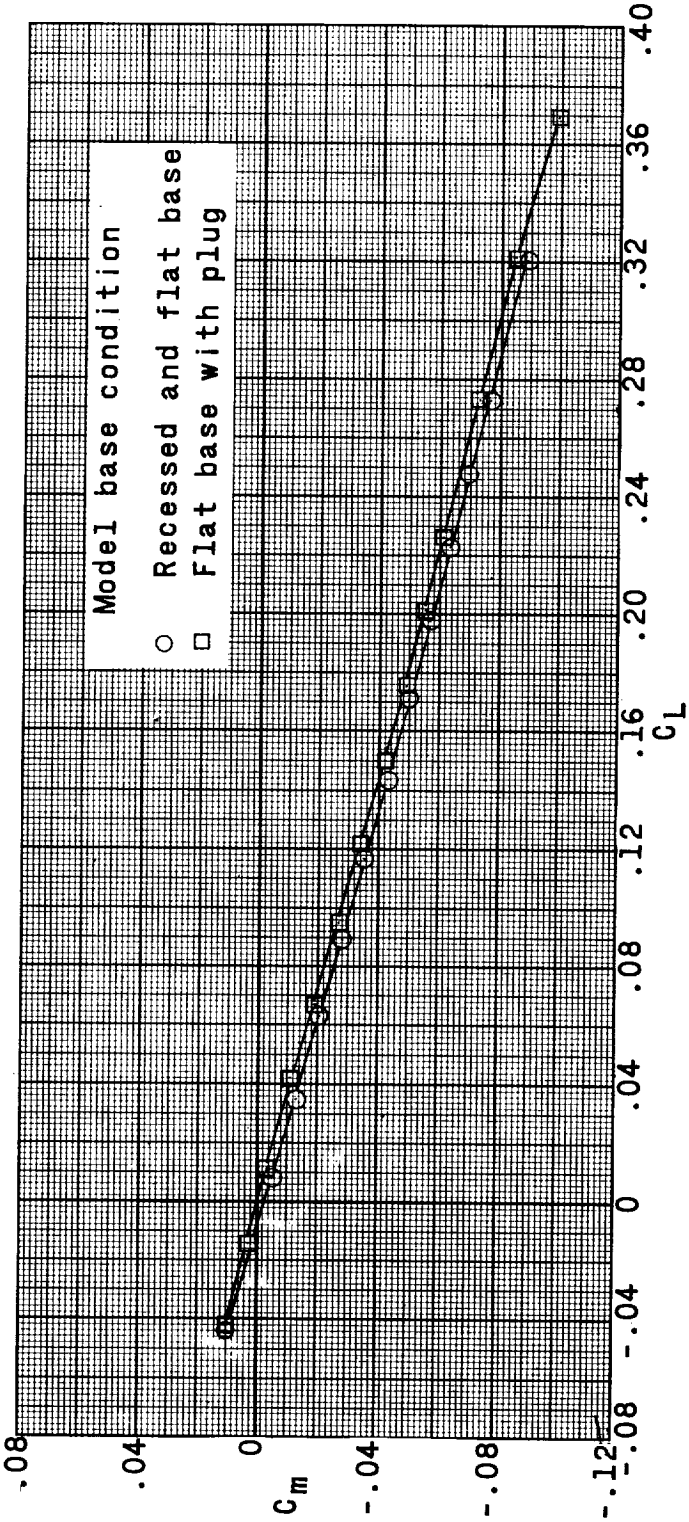

Figure 13.- Effect of base-pressure measuring techniques on longitudinal stability of the B_2W_2 model. M = 2.97.

[redacted]

NASA MEMO 1-24-59L
National Aeronautics and Space Administration.
STATIC LIFT, DRAG, AND PITCHING-MOMENT CHARACTERISTICS OF WINGS WITH ARROW AND MODIFIED-DIAMOND PLAN FORMS COMBINED WITH SEVERAL DIFFERENT BODIES AT MACH NUMBERS OF 2.97, 3.35, AND 3.71. Dennis F. Hasson and John G. Presnell, Jr. January 1959. 50p. diagrs., photos., tab. (NASA MEMORANDUM 1-24-59L) CONFIDENTIAL (Title, Unclassified)

The leading-edge sweep of all wings was about 70.3°. Cambered and uncambered airfoil sections were tested with each plan form. The bodies consisted of a conventional fuselage, a semiconical body, a 3/4-power semibody, and a small body of revolution. All bodies were mounted beneath the wings with the latter three having their apex coincident with the wing apex. Tests were performed through an angle-of-attack range of approximately -4° to 12°. The test Reynolds numbers were approximately 2 x 10^6 and 3 x 10^6 for the models with arrow- and diamond-plan-

Copies obtainable from NASA, Washington (over)

1. Wing-Fuselage Combinations - Airplanes (1.7.1.1.1)
2. Wing-Body Combinations - Missiles (1.7.2.1.1)
3. Stability, Longitudinal - Static (1.8.1.1.1)

I. Hasson, Dennis F.
II. Presnell, John G., Jr.
III. NASA MEMO 1-24-59L

NASA

[redacted]

[redacted]

NASA MEMO 1-24-59L
National Aeronautics and Space Administration.
STATIC LIFT, DRAG, AND PITCHING-MOMENT CHARACTERISTICS OF WINGS WITH ARROW AND MODIFIED-DIAMOND PLAN FORMS COMBINED WITH SEVERAL DIFFERENT BODIES AT MACH NUMBERS OF 2.97, 3.35, AND 3.71. Dennis F. Hasson and John G. Presnell, Jr. January 1959. 50p. diagrs., photos., tab. (NASA MEMORANDUM 1-24-59L) CONFIDENTIAL (Title, Unclassified)

The leading-edge sweep of all wings was about 70.3°. Cambered and uncambered airfoil sections were tested with each plan form. The bodies consisted of a conventional fuselage, a semiconical body, a 3/4-power semibody, and a small body of revolution. All bodies were mounted beneath the wings with the latter three having their apex coincident with the wing apex. Tests were performed through an angle-of-attack range of approximately -4° to 12°. The test Reynolds numbers were approximately 2 x 10^6 and 3 x 10^6 for the models with arrow- and diamond-plan-

Copies obtainable from NASA, Washington (over)

1. Wing-Fuselage Combinations - Airplanes (1.7.1.1.1)
2. Wing-Body Combinations - Missiles (1.7.2.1.1)
3. Stability, Longitudinal - Static (1.8.1.1.1)

I. Hasson, Dennis F.
II. Presnell, John G., Jr.
III. NASA MEMO 1-24-59L

NASA

[redacted]

[redacted]

NASA MEMO 1-24-59L
National Aeronautics and Space Administration.
STATIC LIFT, DRAG, AND PITCHING-MOMENT CHARACTERISTICS OF WINGS WITH ARROW AND MODIFIED-DIAMOND PLAN FORMS COMBINED WITH SEVERAL DIFFERENT BODIES AT MACH NUMBERS OF 2.97, 3.35, AND 3.71. Dennis F. Hasson and John G. Presnell, Jr. January 1959. 50p. diagrs., photos., tab. (NASA MEMORANDUM 1-24-59L) CONFIDENTIAL (Title, Unclassified)

The leading-edge sweep of all wings was about 70.3°. Cambered and uncambered airfoil sections were tested with each plan form. The bodies consisted of a conventional fuselage, a semiconical body, a 3/4-power semibody, and a small body of revolution. All bodies were mounted beneath the wings with the latter three having their apex coincident with the wing apex. Tests were performed through an angle-of-attack range of approximately -4° to 12°. The test Reynolds numbers were approximately 2 x 10^6 and 3 x 10^6 for the models with arrow- and diamond-plan-

Copies obtainable from NASA, Washington (over)

1. Wing-Fuselage Combinations - Airplanes (1.7.1.1.1)
2. Wing-Body Combinations - Missiles (1.7.2.1.1)
3. Stability, Longitudinal - Static (1.8.1.1.1)

I. Hasson, Dennis F.
II. Presnell, John G., Jr.
III. NASA MEMO 1-24-59L

NASA

[redacted]

[redacted]

NASA MEMO 1-24-59L
National Aeronautics and Space Administration.
STATIC LIFT, DRAG, AND PITCHING-MOMENT CHARACTERISTICS OF WINGS WITH ARROW AND MODIFIED-DIAMOND PLAN FORMS COMBINED WITH SEVERAL DIFFERENT BODIES AT MACH NUMBERS OF 2.97, 3.35, AND 3.71. Dennis F. Hasson and John G. Presnell, Jr. January 1959. 50p. diagrs., photos., tab. (NASA MEMORANDUM 1-24-59L) CONFIDENTIAL (Title, Unclassified)

The leading-edge sweep of all wings was about 70.3°. Cambered and uncambered airfoil sections were tested with each plan form. The bodies consisted of a conventional fuselage, a semiconical body, a 3/4-power semibody, and a small body of revolution. All bodies were mounted beneath the wings with the latter three having their apex coincident with the wing apex. Tests were performed through an angle-of-attack range of approximately -4° to 12°. The test Reynolds numbers were approximately 2 x 10^6 and 3 x 10^6 for the models with arrow- and diamond-plan-

Copies obtainable from NASA, Washington (over)

1. Wing-Fuselage Combinations - Airplanes (1.7.1.1.1)
2. Wing-Body Combinations - Missiles (1.7.2.1.1)
3. Stability, Longitudinal - Static (1.8.1.1.1)

I. Hasson, Dennis F.
II. Presnell, John G., Jr.
III. NASA MEMO 1-24-59L

NASA

[redacted]

NASA MEMO 1-24-59L

form wings, respectively. The report also includes an appendix which gives a comparison of techniques for measuring base pressure.

Copies obtainable from NASA, Washington

CONFIDENTIAL

NASA MEMO 1-24-59L

form wings, respectively. The report also includes an appendix which gives a comparison of techniques for measuring base pressure.

Copies obtainable from NASA, Washington

CONFIDENTIAL

NASA

NASA MEMO 1-24-59L

form wings, respectively. The report also includes an appendix which gives a comparison of techniques for measuring base pressure.

Copies obtainable from NASA, Washington

CONFIDENTIAL

NASA MEMO 1-24-59L

form wings, respectively. The report also includes an appendix which gives a comparison of techniques for measuring base pressure.

Copies obtainable from NASA, Washington

CONFIDENTIAL

NASA

NASA MEMO 1-24-59L

form wings, respectively. The report also includes an appendix which gives a comparison of techniques for measuring base pressure.

Copies obtainable from NASA, Washington

CONFIDENTIAL